A new simpler way to obtain high fusion power gain in tandem mirrors

2017 Nucl. Fusion 57 056014

(http://iopscience.iop.org/0029-5515/57/5/056014)

IOP Publishing | International Atomic Energy Agency Nuclear Fusion

Nucl. Fusion **57** (2017) 056014 (20pp) https://doi.org/10.1088/1741-4326/aa5e54

A new simpler way to obtain high fusion power gain in tandem mirrors

T.K. Fowler[1], R.W. Moir[2] and T.C. Simonen[3]

[1] University of California, Berkeley, CA, United States of America
[2] Vallecitos Molten Salt Research, Livermore, CA, United States of America
[3] Berkeley, CA, United States of America

E-mail: Simonen42@yahoo.com

Received 26 July 2016, revised 17 January 2017
Accepted for publication 31 January 2017
Published 24 March 2017

Abstract

From the earliest days of fusion research, Richard F. Post and other advocates of magnetic mirror confinement recognized that mirrors favor high ion temperatures where nuclear reaction rates $\langle\sigma v\rangle$ begin to peak for all fusion fuels. In this paper we review why high ion temperatures are favored, using Post's axisymmetric Kinetically Stabilized Tandem Mirror as the example; and we offer a new idea that appears to greatly improve reactor prospects at high ion temperatures. The idea is, first, to take advantage of recent advances in superconducting magnet technology to minimize the size and cost of End Plugs; and secondly, to utilize parallel advances in gyrotrons that would enable intense electron cyclotron heating (ECH) in these high field End Plugs. The yin-yang magnets and thermal barriers that complicated earlier tandem mirror designs are not required. We find that, concerning end losses, intense ECH in symmetric End Plugs could increase the fusion power gain Q, for both DT and Catalyzed DD fuel cycles, to levels competitive with steady-state tokamaks burning DT fuel. Radial losses remain an issue that will ultimately determine reactor viability.

Keywords: tandem mirror, advanced fuel, mirror reactor, axi-symmetric magnetic mirror, fusion reactor concept

(Some figures may appear in colour only in the online journal)

1. Introduction

This paper draws attention of mirror specialists and the wider fusion community to a new idea utilizing advances in magnet technology that potentially make tandem mirrors a viable candidate to burn advanced fuels in the future, and also improves performance for deuterium–tritium (DT) fuel in the nearer term. This is not intended to be a research paper in depth but instead relies on simple estimates to show why the new idea is plausible, with illustrative examples of reactor parameters, and concluding with subjects for further study.

The version of the tandem mirror considered here is a variation on the axisymmetric kinetically stabilized tandem mirror (KSTM) invented by Post [1–3], using design concepts first elucidated by Mirnov and Ryutov [4, 5], now confirmed in the gas dynamic trap (GDT) experiment in Novosibirsk [6, 7]. While the earliest tandem mirror experiments used asymmetric minimum-B (yin-yang/Baseball) magnetic wells as the certain way to stabilize End Plugs against MHD instability, Post's KSTM uses only circular coils giving the axisymmetric coil geometry sketched in the upper half of figure 1. In this design, MHD stability is provided by the favorable curvature of magnetic field lines in the Expander where flux diverges as it emerges from the last mirror coil.

In the tandem mirror, the End Plugs serve only to prevent leakage out of the ends of the straight solenoid in figure 1, while the solenoid itself serves as the reactor [8, 9]. The solenoidal reactor is called the Center Cell. Fusion energy produced as charged particles escapes out the ends along expanding magnetic field lines that spread the power over a large area in the Expander, shown in more detail in figure 2. Fusion energy produced as radiation and neutrons is captured in the blanket shown in figure 3. Ignition in the Center Cell is achieved by mirror machines serving as End Plugs in figure 1. Faster end leakage of electrons compared to ions creates an electrostatic potential positive in the mirrors relative to end

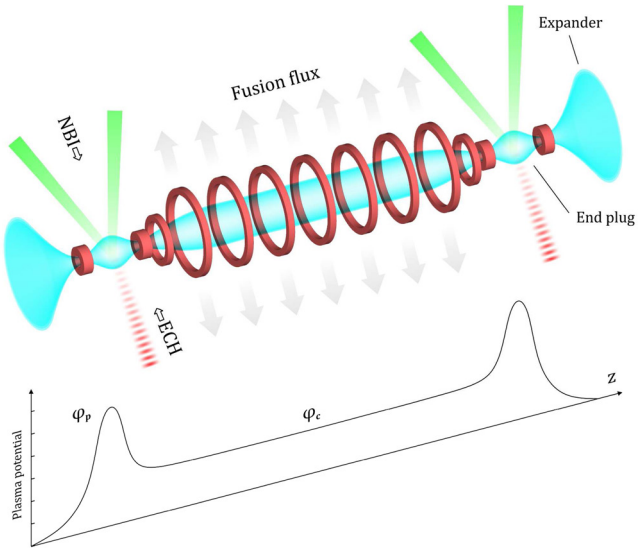

Figure 1. Axisymmetric coil geometry sketched in the upper half and electrostatic confining potential Φ_c in the lower half.

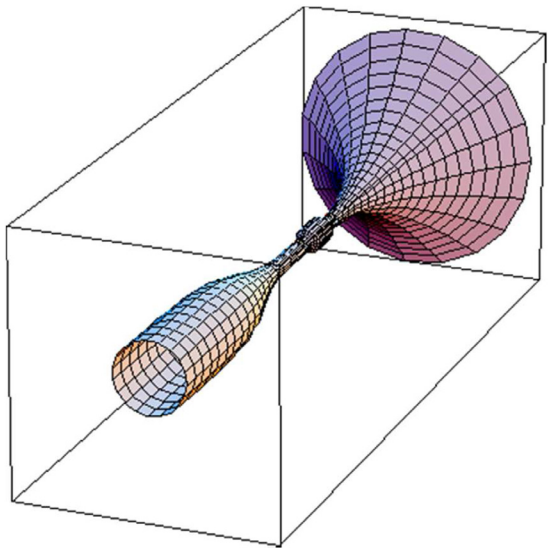

Figure 2. The Expander isolates hot electrons from the end walls, stabilizes the plasma column and guides escaping plasma to the direct converter.

walls and relative to the Center Cell. The resulting potential profile along the length of the machine is sketched in the lower half of figure 1. That Φ_c is less than Φ_p serves to confine ions in the Center Cell. In the original tandem mirror concept, confirmed in the TMX experiment [10], the peaks in potential were created solely by neutral beams depositing fast ions in the end plugs. Here we add electron cyclotron heating (ECH), as shown.

Besides the evident engineering advantages of the linear blanket geometry in figure 3, tandem mirrors should be able to achieve a plasma pressure parameter $\beta \approx 1$, which greatly reduces required magnetic field strengths in the Center Cell. And, for an ignited Center Cell, the End Plug power required to maintain ignition is fixed, giving a fusion power gain $Q \propto L_C$, the length of the Center Cell.

The main disadvantage has been lagging performance of tandem mirrors compared to tokamaks, due in part to ion cooling by collisions with electrons at the low electron temperatures achievable in small devices; but also due to the appearance of radial transport when end plugging is most successful. We find that the key to reactor-level performance in tandem mirrors lies in new technology that improves end plugging and appears to stabilize at least some of the instabilities responsible for poor performance in the past. First and foremost is the potential for complete stabilization of ion cyclotron modes in the End Plugs, made possible with little power expenditure due to the advent of high field superconductors already producing 27 tesla fields in steady state [12], in coils with small dimensions (order 1 m), similar to dimensions of the compact, theoretically-stable End Plugs of our reactor model in section 7. Second is ECH enhancement of end plugging without resorting to so-called thermal barriers utilizing mirror-confined electrons that probably contributed to instability.

Advances in gyrotrons in parallel with advanced superconductors allow us to apply ECH at the high fields that stabilize ion cyclotron modes. The net result is tandem mirror performance limited only by the radial losses due to thermal gradients and trapped particles as in tokamaks, with some possibility of controlling these processes by end plates not available in toroidal devices, and feedback applied only to the small End Plugs. Given adequate control of radial losses, in section 7 we give examples of reactors with much less magnetic energy storage than tokamaks, even for reactors employing the Catalyzed DD fuel cycle.

In undertaking this paper, our goal has been to use simple estimates to show that most issues concerning end plugging could be calculated from first principles in an actual design, in contrast with scaling laws of radial transport losses that still may be required in the Center Cell, as in tokamaks. The remainder of this paper is organized as follows. Section 2 discusses radial confinement in the Center Cell of tandem mirror reactors. Section 3 discusses the new idea for end plugging using strong ECH heating and the role of the magnetic Expander in preventing heat loss to the end walls. Section 4 discusses the role of the Expander in stabilizing the End Plugs, including a discussion of trapped particle modes. Section 5 discusses End Plug stability at ion cyclotron frequencies and how this determines the minimum plasma radius. Section 6 discusses why tandem mirrors favor reactors at high ion temperatures allowing consideration of advanced fuels, with examples in section 7. Section 8 suggests experiments that would give definitive answers to issues of end plugging. Section 9 lists some subjects for further study by theory, simulations and engineering. Section 10 gives the summary including an assessment of how well the above goals have been fulfilled. Appendix A discusses pros and cons for advanced fuels, and appendix B discusses direct conversion to electricity.

We have not attempted to do a complete review of mirror research. Only references that we find to be most relevant to our new idea are included. More complete lists can be found in Post's 1987 review of mirror research [13] and a more recent report in [14].

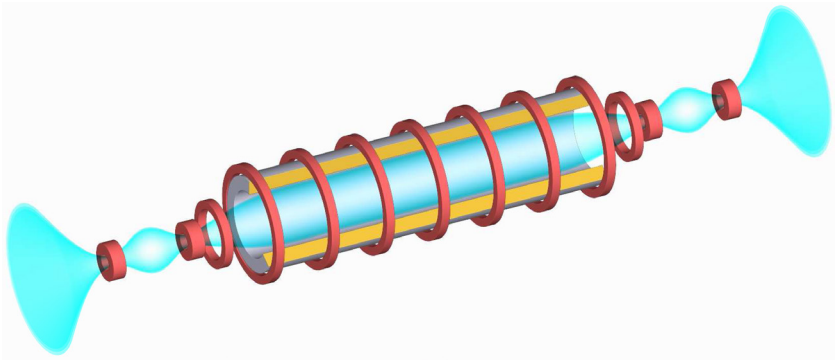

Figure 3. Fusion energy produced as radiation and neutrons is captured in the blanket.

2. Radial losses in the Center Cell

When end-plugging is successful, the tandem mirror Center Cell becomes the equivalent of the theorist's idealized straight tokamak, without the current (though an axial current providing magnetic shear could be added with little effect on end plugging). Thus, conceptually, the tandem mirror Center Cell is neither better nor worse than tokamaks concerning radial transport, except for three unique features.

On the downside, electrons and ions isolated by trapping in mirrors and potential wells exceed trapping by toroidal curvature in tokamaks, though spherical tokamaks also have many trapped particles. Trapped particle modes are discussed in section 4.2.

Potentially on the upside is freedom to adjust radial profiles in regimes in which end losses dominate over radial losses. Unlike tokamaks in which radial gradients must exist everywhere to eject heat, we will find that, when end losses dominate, both the density and temperatures in the KSTM Center Cell can assume flat profiles, bounded by a tokamak-like 'pedestal' where any radial transport occurs. We will return to this point in section 7.5 that discusses the mapping of End Plug magnetic profiles to the pedestal, and in section 7.7 that discusses results of 1D simulations of radial transport (SYMTRAN) that verified flat profiles in the Center Cell interior [15], showing also how diffusion by electron temperature gradient (ETG) turbulence might be tolerable inside the pedestal.

The other unique feature is access from the ends to apply radial electric fields across the pedestal, shown to affect radial transport in the Macrator Electric Tokamak at UCLA [16]. The open ends in tandem mirrors allow the introduction of segmented end plates at reactor scale, with an array of voltages externally controllable. Evidence to date has shown some success in using segmented end plates to control neoclassical radial losses due to asymmetric minimum-B end plugs, in the TMX-U experiment [17]. But also the TARA tandem mirror experiment showed clear evidence of trapped particle modes similar to those in tokamaks [18].

In section 4 we will confirm Post's idea of preventing MHD instability by kinetic stabilization, leaving control of trapped particle modes in the End Plugs and electron temperature gradient (ETG) modes in the Center Cell as the main uncertainties. Trapped particle instability is discussed in section 4.3. As tokamak history shows, ETG transport probably cannot be assessed until sufficiently stable End Plugs are achieved to warrant extension to a full scale tandem mirror. How to design and test stable axisymmetric End Plugs yielding attractive tandem mirror reactors is the focus of this paper.

3. How strong ECH improves end plugging

Because particle energies of escape out the ends are determined by potentials rather than temperatures, plasma confinement in tandem mirrors is best described by the ion particle confinement time for end loss in the Center Cell. Ignoring radial loss, the ion particle lifetime in the Center Cell is given by the following formula due to Pastukhov [19]:

$$n_c\tau_i = n_c\tau_{ii}(\Phi_i/T_{ic})\exp(\Phi_i/T_{ic}) \tag{1a}$$

$$\Phi_i = \Phi_p - \Phi_c = T_{ep}\ln(n_p/n_c) \tag{1b}$$

Here and hereafter, labels p and c refer to the End Plug and Center Cell, respectively, and both temperatures (T's) and potentials (Φ's) are in energy units. The potential Φ_i confining ions in the Center Cell is the difference in potential between the End Plug and the Center Cell in figure 1, due to a difference in End Plug density n_p and Center Cell density n_c. For end losses, energy confinement is accounted for by assigning an energy loss Φ_p per ion–electron pair for hydrogenic fuel, while typically highly-charged heavy ions are lost radially.

Note that it is the electron temperature T_{ep} in the End Plugs that determines axial confinement, through $\Phi_i \propto T_{ep}$ in equation (1*b*). In the original tandem mirror concept, T_{ep} was determined by electron heating by the ions, typically yielding $T_{ep} < 0.1\ E_o$ for a beam energy E_o [20]. It was this that prompted initial research on 1 MeV neutral beams as a technology for tandem mirrors, now being brought to fruition in technology development for the international thermonuclear experimental reactor (ITER) [21]. It was also the absence of MeV beams in the early days that prompted the thermal barrier concept as a way to achieve high $T_{ep} \gg T_{ec}$ by ECH heating [22].

The new idea here is to recognize that intense ECH heating can create $T_{ep} \gg T_{ec}$ while avoiding the mirror-confined electrons essential to creating thermal barriers, and to combine this with the MeV beams now being developed for ITER as the best way to achieve MeV potentials in Post's KSTM End

Plugs. A definitive experimental test of this idea is our highest priority in section 8, while more theory and design of ECH end plugging tops our list of subjects for further study in section 9. Here we show why achieving $T_{ep} \gg T_{ec}$ should be feasible.

3.1. Experimental evidence

Why achieving $T_{ep} \gg T_{ec}$ is possible has historical roots in the first attempt to use ECH to create a target plasma for ion beam injection. This was the original goal of the ELMO experiment initiated in the early 1960s at the Oak Ridge National Laboratory [23]. This experiment—repeated in many subsequent mirror facilities—showed that modest ECH power can both create a plasma by breakdown of gas and heat a portion of the plasma electrons to enormous energies (1 kW producing 100's of keV in a 1 liter volume, or 1 MW m^{-3}).

The hot electrons in ELMO were mirror-confined, with $T_{e\perp} \gg T_{e\|}$. Mirror- trapped electrons drive the plasma potential negative, as in thermal barriers [22]. The T_{ep} in equation (1*b*) must be thermal. Delineating the conditions for thermalization of hot electrons is the main theoretical contribution of this paper, in section 3.2. That most experiments to date violate these conditions adds motivation for the Next Step experiment discussed in section 8.

3.2. Theory: electron runaway

A detailed study of ECH heating in an End Plug, involving both Fokker–Planck calculations of ion and electron scattering and ECH propagation and absorption, is beyond our scope and rises to the top of our list of subjects for further study in section 9. However, we find that the main points are subject to simple analysis, as follows.

Runaway heating of electrons to very high energies is not in dispute, having been demonstrated in many experiments including GAMMA 10 [24]. That runaway is possible follows from the fact that the ECH heating rate tends to increase with increasing electron energy while the cooling rate decreases. Because the electron-electron scattering rate depends on the highest energy electrons, runaway heating from a cold electron bath occurs at the same rate independent of the temperature of the bath (hence the ability to create hot electrons in ELMO). Noting that the 250 keV electrons of interest are only at the threshold of relativistic effects, we use the following approximate non-relativistic equation including the points above:

$$dT_{ep}/dt = E^* - (n_c T_{ep}/n\tau_{ee}) \quad (2a)$$

$$E^* = eE_{RF}v_e \quad (2b)$$

$$n\tau_{ee} = 4 \times 10^{14} T_{ep}^{3/2} \quad (2c)$$

$$E_{RF} > (n_c T_{ep}/ev_e n\tau_{ee}) \propto (n_c/T_{ep}) \quad \text{runaway} \quad (2d)$$

Here and hereafter we use SI units. The electron velocity v_e arises from the RF heating rate E^* at the fundamental resonance, giving $(eE_{RF}\rho_e\omega_{ce}) = eE_{RF}v_e$ with Larmor radius ρ_e and cyclotron frequency ω_{ce}, (valid relativistically). Solving equation (2*a*) in steady state gives the runaway condition in equation (2*c*), where on the right hand side we take $v_e \propto T_{ep}^{1/2}$ while in the relativistic limit $E_{RF} \propto 1/T_{ep}^{1/2}$.

We see that in startup n_c and T_{ep} must rise together to avoid thermal collapse on the one hand or excessive heating on the other hand. We defer startup to section 9.1, Item (3), where we recommend more research on startup using improved versions of the SYMTRAN code [15], with the expectation that equation (2*d*) insures thermal stability. In the remainder of the paper we only require the ECH power in steady state. This power is just that satisfying the runaway condition at the final hot electron temperature T_{ep}. We obtain:

$$P_{ECH} = V_P n_p n_c 3/2 (T_{ep} - T_{ec})/(n\tau_{ee}) \quad (3a)$$

$$\approx 3200 V_P (n_{p20} n_{c20}) [(T_{ep} - T_{ec})/T_{ep}^{3/2}] \quad \text{MW} \quad (3b)$$

Equation (3*a*) is the right hand side of equation (2*a*) set equal to zero and integrated on energy and volume with weighting $f_e(E)$, the electron energy distribution. The right hand side of equation (3*a*) is the cooling rate with $n\tau_{ee}$ in equation (2*c*). The cooling is proportional to $n_p n_c$, the product of the hot and cold electron populations in the plug. The cold population visiting from the Center Cell has a density $n_p \exp[-(\Phi_i/T_{ep})] = n_c$ (the Center Cell density). In equation (3*b*), $n_{20} = (n/10^{20})$ in SI units, with T_{ep} in keV here and hereafter.

3.3. Theory: electron thermalization

Electron heating can be approximated by the following 1D Fokker–Planck equation for electrons in the End Plug, written in terms of the electron energy E [25]:

$$-\partial(F - E^*)f_1/\partial E + \partial^2(EDf_1)/\partial E^2 - f_1/\tau_1 = 0 \quad (4a)$$

$$f = f_1 + f_C + f_p \equiv + f_1(E) + C_c \exp(-E/T_{ec}) + C_p \exp(-E/T_{ep}) \quad (4b)$$

$$-\partial(F - E^*)f_1/\partial E = f_1/\tau_1 \quad \text{runaway} \quad (4c)$$

$$(\tau_{ii}/\tau_{ee}) \approx (m_i/m_e)^{1/2}(E_o/T_{ep})^{3/2} \approx 40(E_o/T_{ep})^{3/2} \gg 1 \quad (4d)$$

Here E^* is the ECH heating from equation (2*b*). Runaway is represented by collisional friction $F(E) < E^*$ above some energy $E_1 > T_{ec}$, giving also diffusion $D < E^*$ so that f_1 becomes the solution of equation (4*c*).

Because resonance zones are localized, accelerated electrons bouncing between mirrors visit and experience collisions in non-resonant regions. Following Cohen [26], we account for this by dividing the electron distribution into, in this case, three parts, whereby electrons visiting from the Center Cell (f_c) feed ECH-heated electrons (f_1) which in turn feed an energetic, potential-trapped population (f_p) at a rate f_1/τ_1 representing loss of resonance when ECH-heated electrons suffer a collision when visiting non-resonant zones. Without knowing details, we can see that the outcome would be determined by the rate $\tau_1 \approx \tau_{ee}$ (the electron collision time) in comparison with the lifetime τ_{ii} for stable mirror-confined ions that must equal the overall lifetime of electrons. Then,

since $\tau_{ii} \gg \tau_1 \approx \tau_{ee}$, most of the electrons will accumulate in f_p before escaping, whereby f_p becomes the dominant population (f_c being smaller by a factor $n_c/n_p \approx 1/5$).

The condition for f_p to Maxwellize and become dominant is shown in equation (4*d*). Introducing a typical value $T_{ep} = 1/4\ E_o$ for neutral beam energy E_o, we obtain $(\tau_{ii}/\tau_{ee}) \approx 300$ as the number collisions before escaping, which we derate to 200 in anticipation of ion collisional effects discussed in section 7. With 200 collisions before escaping, electrons in f_p are well thermalized, and the residual high energy tail is small, of order $f_1 \approx \exp(-\Phi_p/T_{ep})f_p \approx 0.01\, f_p$.

3.4. Electron instabilities

The dominance of f_p over f_1 eliminates temperature anisotropy as the source of free energy, perhaps the origin of instability in mirror-confined electrons in TARA, GAMMA-10 and also the ELMO bumpy torus (EBT) [27]. To the extent that the electron energy distribution becomes dominated by f_p in equation (4*b*), the electron Vlasov distribution in the laboratory reference frame becomes $f(\mathbf{x},\mathbf{v}) \propto \exp(-\varepsilon/T)$ with $\varepsilon = 1/2\ m_e v^2 - e\Phi$. This or any distribution monotonically decreasing with ε is well known to be stable acting on itself, leaving electron drift waves (ETG, trapped particle, DCLC), discussed in later sections, as the phenomena of interest.

3.5. Eliminating energy loss by secondary electrons

A point perhaps not yet appreciated by the wider fusion community is that the low electron temperatures in early tandem mirrors (<250 eV) were to be expected due to the necessity to stabilize DCLC modes by streams that cooled the plasma dramatically. How increasing the End Plug plasma radius stabilizes DCLC is discussed in section 5. Here we make the separate point that secondary electrons at the end walls, which also contributed to low electron temperatures in the past, can be eliminated by the KSTM Expander in figure 2, which also stabilizes MHD activity in the End Plugs.

The criterion for eliminating secondaries, derived by Ryutov [11] and confirmed in the GDT experiment [6, 7], can be understood as follows. Thermal isolation of the plug electrons from secondaries and other end wall effects occurs when a finite $\partial\Phi/\partial z$ is no longer needed to maintain ambipolar flow. This establishes a 'quiet zone' at the wall where the electric field is essentially zero so that secondary electrons emitted at the end wall that plagued earlier mirror experiments are either suppressed at the outset or can be absorbed or deflected by cold plasma that is itself confined to the wall region by the large potential near the mirrors.

We estimate the length L_{qz}, beyond which the quiet zone exists, as follows. Ions cease to be confined beyond the final mirror, giving an escaping current $j_i = en_{mirror}v_i$. Electron confinement extends beyond the mirror to the point where $\partial\Phi/\partial z = 0$ and the quiet zone begins. Because electrons are quasi-Maxwellian due to confinement by the ions, the fraction escaping at the mirror is of order $\exp(-e\Phi_{mirror}/T_e)$ which is also the ratio of the density at the electron escape point to that at the mirror throat. This density ratio is also determined by magnetic flux expansion that also gives $j_i \propto B(z)$ to conserve ion current and magnetic flux. Because scattering already imparts an energy $\approx E_o$ to escaping ions, their velocity parallel to **B** is almost constant in the expander so that $j_i \propto n \propto B(z)$, giving $n = n_{mirr}/K_M = n_{mirr}\exp[-(\Phi_{mirr}/T_{ep})]$ as the electron density where electrons escape. Then the fraction of the electron density escaping at the mirror is $\exp[-(\Phi_{mirr}/T_{ep})]_{mirr} = 1/K_M$, giving, for ambipolar outflow, $j_e = -e(n_{mirr}/K_M)v_e = -j_i = -en_{mirr}v_i$; hence [11]:

$$K_M = (B_{mirr}/B) = v_e/v_i \tag{5a}$$

$$(L_{qz}/(L_{mag}/\sqrt{R_M}))^N = (T_{ep}/E_o)^{1/2}(m_i/m_e)^{1/2} \tag{5b}$$

$$L_{qz} \approx (m_i/m_e)^{1/2N}L_{mag} \approx 4L_{mag} \tag{5c}$$

In equation (5*a*), B is a function of L_{qz}. In equation (5*b*), R_M is again the mirror ratio in the end plug while in equation (5*a*) K_M is the mirror ratio from the mirror throat to the quiet zone at a distance L_{qz}. In equation (5*b*), we approximate $B_z(z) \propto (L_{mag}/z)^N$ in the field beyond the mirror coils, with maximum $N = 3$ for the flaring field lines of the dipole field beyond the final mirror, and a smaller N if shaping of the field is required, down to a minimum $N = 2$ representing straight field lines. Equation (5*c*) gives $L_{qz} = 4L_{mag}$ for $N = 3$, equaling 3 m or so depending on coil dimensions, indicating that it should be possible to design so as to initiate the quiet zone near the mirrors, leaving most of the expander volume to serve as a kinetic stabilizer and divertor, and also as a Direct Converter as discussed in appendix B.

3.6. ECH plugging: summary

We conclude that the key to generating high End Plug potentials with ECH is good confinement of the ions that in turn confine the electrons well enough for them to become thermalized. The main requirements are that heat drain by secondary electrons be eliminated, using the magnetic Expander as discussed in section 3.5, and that all ion cyclotron instabilities be eliminated by design, discussed in section 5.

The main point is that good end plugging by ECH is only possible in an End Plug of sufficient radius, using neutral beams of sufficient energy. A sufficient radius is required to eliminate the drift cyclotron loss cone (DCLC) instability. A sufficient beam energy is required to confine electrons for many collision times by equation (4*d*) with the classical ion confinement time applicable if DCLC (and other ion modes) are eliminated. To our knowledge no experiment to date has met all of these conditions. Our reactor cases in section 7 and the Next Step experiment discussed in section 8 do meet these conditions. Residual trapped particle modes are discussed in section 4.2.

4. Stability: MHD and trapped particle modes

In this Section, we review Post's kinetic stabilization of symmetric tandem mirrors using the same magnetic Expander that was found to isolate hot electrons from the end walls, in section 3.5, and potential problems concerning trapped particle modes and how that might be prevented.

4.1. Kinetic stabilization of axisymmetric end plugs

Like tokamaks, tandem mirrors apply average-minimum B to stabilize MHD interchange. In the TMX and TMX-U tandem mirror experiments, End Plug stability was provided by Baseball coils producing asymmetric mirror fields. But research on these devices soon disclosed non-ambipolar neoclassical losses due to orbital drifts in the asymmetric field [28], thereby adding incentive to return to axisymmetric mirrors matching the axisymmetry of the Center Cell.

Several ways to stabilize axisymmetric mirrors have been explored including stabilization by pressure in an expander in anticipation of Post's kinetic stabilizer [29–31]. A breakthrough occurred when the GDT experiment confirmed stabilization by the pressure of escaping plasma in the expander that also served to isolate hot electrons from the end walls. It was the results in GDT that prompted Post to propose his kinetic stabilizer, as follows.

We write the condition for average-minimum B stabilization at low plasma pressure compared to the magnetic pressure (low β) as [3]:

$$(\gamma_{\mathrm{MHD}})^2 \propto \int_{-L}^{L} \mathrm{d}z R(z)^3 (d^2R/dz^2) p(z) > 0 \tag{6}$$

where γ_{MHD} is the MHD growth rate; $R(z)$ is the radius conserving magnetic flux in a changing magnetic field; $(d^2R/\mathrm{d}z^2)^{-1}$ is the magnetic radius of curvature; and $p(z)$ is the plasma pressure, in the End Plug and in the magnetic Expander. We can divide equation (6) into two parts:

$$\int_0^{L\mathrm{stab}} \mathrm{d}z R(z)^3 (d^2R/\mathrm{d}z^2) p_{\mathrm{stab}} > L_{\mathrm{p}} n_{\mathrm{p}} (E_{\mathrm{o}} + T_{\mathrm{ep}}) R_{\mathrm{p}}^3 (4R_{\mathrm{p}}/L_{\mathrm{p}}^2) \tag{7}$$

Here the left hand side with good curvature represents the Expander over a length L_{stab} beginning at the beginning of the quiet zone in section 3.5. The right hand side is the unstable End Plug (or roughly double this to include the connection between the solenoid in a tandem mirror: see section 7.5). The pressure profile is determined by neutral beam injection (NBI) giving n_{p} in the End Plug, and in Post's scheme by low energy beams of heavy ions in the Expander, specially provided as a way to add pressure in the Expander when good confinement limits outflow from the End Plugs to the end walls.

Post and colleagues have solved equation (6) using the FLORA code and find stable conditions with a stabilizer power comparable to End Plug power, in a length L_{stab} about 4 times longer than the End Plug [3], similar to L_{qz} in equation (5*c*), and optimally located at $L_{\mathrm{qz}} < z < (L_{\mathrm{qz}} + L_{\mathrm{stab}})$ so as to avoid acceleration by $\nabla\Phi$ near the mirror that wastes ECH power (ions accelerated by $\nabla\Phi$ get their energy from the deceleration of electrons heated by ECH). Why injecting heavy ions is essential to obtain a short stabilizer can be understood as follows. Given p_{stab} that works, the required stabilizing power P_{stab} is given by:

$$P_{\mathrm{stab}} = (v_{\mathrm{stab}}/L_{\mathrm{stab}}) \int_{\mathrm{stab}} \mathrm{d}z R(z)^2 p_{\mathrm{stab}} \tag{8}$$

where we integrate over the stabilizer only and v_{stab} is the velocity of stabilizer ions fixed by the beam that injects them. We apply the paraxial approximation for B_z giving [20]:

$$\begin{aligned} B_z(r,z) &= r^{-1}\partial(rA_\phi)/\partial r \\ &= B_z(0,z) - 1/4R^2(d^2B_z(0,z)/\mathrm{d}z^2) + \ldots \end{aligned} \tag{9a}$$

$$B_z(0,z) = \left(B_{\mathrm{p}}/R_{\mathrm{M}}\right)\left(L_{\mathrm{mag}}/z\right)^N \text{ Expander} \tag{9b}$$

$$R(z) = \left(R_{\mathrm{p}}/\sqrt{R_{\mathrm{M}}}\right)\left(z/L_{\mathrm{mag}}\right)^{N/2} \text{ Expander} \tag{9c}$$

Here $N = 3$ representing a dipole field gives the curvature at the end of a simple mirror, while $N = 2$ represents applying colis to straighten out the field lines some distance from the mirror. The point we wish to make here is that, taking $N = 3$ as an example, for more or less any $p(z)$ profile filling the stabilizer region, determining the magnitude of $p(z)$ required for stability and substituting the resulting $p(z)$ into equation (8) gives constant $(v_{\mathrm{stab}}/L_{\mathrm{stab}}^2)$, hence:

$$L_{\mathrm{stab}} \propto \sqrt{v_{\mathrm{stab}}} \propto \sqrt{(T_{\mathrm{stab}}/A)} \tag{10}$$

Hence the power is low only if T_{stab} is small (<1 keV) and the beam atomic number A is large. For this reason, Post chose to inject Cs from the ends, though this may not be compatible with other uses of the Expander, as discussed in appendix B.

4.2. Trapped particle modes

Any device stabilized by average minimum B is subject to ballooning instability that bends field lines and hence occurs at high $\beta \propto p/B^2$ (perhaps unlikely in tandem mirrors [20]), and trapped particle modes that do not bend field lines and hence can occur even at low β. We follow Berk and Pratt [32] who analyzed Post's scheme using the trapped particle formalism of Berk and Lane [33]. Their criterion for stabilizing $m = 1$ modes applied to our design gives:

$$(\omega^* \Delta Q)^2 > 4\gamma_{\mathrm{MHD}}^2 (1 + Q) \tag{11}$$

with the definitions:

$$|\omega^* \Delta Q)| = 2\left(eB_{\mathrm{p}}R_{\mathrm{p}}^2\right)(M^*)^{-1} \sum \int_{\mathrm{stab}} \mathrm{d}z R(z)^2 n_{\mathrm{stab}}(z) \tag{12a}$$

$$Q = [(eB_{\mathrm{p}}R_{\mathrm{p}}^2)/\langle T_{\mathrm{stab}}\rangle] \left|\omega^* \Delta Q\right| \tag{12b}$$

$$1/\langle T_{\mathrm{es}}\rangle = \left\{ \left[\sum \int_{\mathrm{exp}} \mathrm{d}z R(z)^2 \left(n_{\mathrm{exp}}(z)/T_{\mathrm{es}}\right) \right] / \sum \int_{\mathrm{stab}} \mathrm{d}z R(z)^2 n_{\mathrm{stab}}(z) \right\} \tag{12c}$$

$$\gamma_{\mathrm{MHD}}^2 = (M^*)^{-1} \sum \int_{-L}^{L} \mathrm{d}z \ [R(z)^3 (d^2R/\mathrm{d}z^2)] \ n_{\mathrm{p}} E_{\mathrm{o}} \tag{12d}$$

$$M^* = \int_{-L}^{L} \mathrm{d}z R(z)^4 n(z) m_{\mathrm{i}} \tag{12e}$$

$$n_{\mathrm{stab}}(z) = \beta_{\mathrm{exp}} (B_{\mathrm{exp}}^2/\mu_{\mathrm{o}} T_{\mathrm{stab}}) \tag{12f}$$

$$\beta_{\mathrm{exp}} = \beta_{\mathrm{p}} (R_{\mathrm{p}}/L_{\mathrm{p}}) (L_{\mathrm{exp}}/R_{\mathrm{exp}}) = (\mu_{\mathrm{o}} n_{\mathrm{p}} E_{\mathrm{o}}/B_{\mathrm{p}}^2) (R_{\mathrm{p}}/L_{\mathrm{p}}) (R_{\mathrm{p}}/z)^{1/2} \tag{12g}$$

$$B_{exp}/B_p = \left(R_p/z\right)^3 ; R(z)/R_p = \left(z/R_p\right)^{3/2}; \left(L_{exp}/R_{exp}\right) \rightarrow \left(R_p/z\right)^{1/2} \tag{12h}$$

where Σ sums over particle species and equation (12*d*) repeats equation (6). Small effects of the End Plug mirror ratio have been omitted for simplicity. In equation (12*a*), we take $n_{stab}(z)$ to be the minimum needed for MHD stabilization in equation (8), giving equation (12*f*) with $L_{exp} \rightarrow z$. In equation (12*d*), we again take the End Plug to be the dominant unstable region and we take γ_{MHD} to be the growth rate with no stabilizer, giving pressure as that of the energetic ions with beam energy E_o.

We do not claim a thorough treatment, but note the following. In equation (12*a*), the stabilizing quantity $|\omega^* \Delta Q)|$ is proportional to $\Sigma \int_{stab} dz R(z)^2 n_{stab}(z)$, which is the number of particles integrated over the stabilizer portion of the expander (designated stab). This same integral appears in our calculation of kinetic stabilizer power in equation (8), indicating a fixed relationship between MHD stability and trapped particle instability that determines the minimum trapped particle stabilization power in ratio to MHD stabilization power. That MHD stability does not guarantee trapped particle stability follows from the favorable extra weighting $(R/R_c) \propto z$ (for $N = 3$) in calculating the Expander contribution to γ^2_{MHD} in equation (12*d*) but absent from the calculation of $|\omega * \Delta Q)|$ in equation (12*a*). We illustrate this as follows.

First we note that $p_{stab} = n_{stab} T_{stab}$ is determined by injection in Post's scheme so that p_{stab} can be removed from the integral in equation (7), allowing us to solve for the minimum n_{stab} giving MHD stability:

$$(n_{stab})_{MHD} > n_p (E_o/T_{stab}) \left[(4R_p^4/L_p) / \int_{stab} R^3 (d^2R/dz^2) \right] \tag{13}$$

Here we evaluated MHD growth due to the End Plug giving $\gamma^2_{MHD} \propto (L_p R_p^3/R_{curv}) = (4R_p^4/L_p)$ using the Sagitta approximation $(d^2R/dz^2) \approx (4R_p/L_p^2)$. Next we multiply by C^* and introduce $n_{stab} = C^*(n_{stab})_{MHD}$ into equation (11) with $Q \gg 1$, typical of our parameters. After some algebra, we obtain:

$$C^* > 2\left(\int_{stab} R^3 (d^2R/dz^2) / \int_{stab} R^2 \right) \approx (L_{stab}/L_{mag}) \gg 1 \tag{14}$$

where L_{stab} is the length of the stabilizer and L_{mag} is the magnetic scalelength in the Expander. Thus, as anticipated, stabilization of trapped particle modes requires much higher n_{stab} in the stabilizer requiring an unacceptable power compared to the plug power that would be sufficient to stabilize MHD, similar to the results of Berk and Pratt [32].

4.2.1. Dissipative sheath instability. Whether trapped particle instability in the KSTM is a fatal flaw depends on the extent to which mass in the Center Cell contributes to slowing down the growth rate to levels that can be controlled by feedback. As an example when feedback works, we consider a different trapped particle instability concerning sheath formation isolating the End Plug from the stabilizer, analyzed by Ryutov [34]. Again we consider only the $m = 1$ mode. Then Ryutov's dispersion relation can be written as:

$$\omega^2 + \gamma^2_{MHD} = -i\omega \gamma_{MHD} (n_{stab}/n_1) \tag{15a}$$

$$n_1 = n_c \left[2(T_{es}/T_{ic})(m_e/m_i)(n_p/n_{stab})(L_p/L_c) \right] \tag{15b}$$

$$Im\omega \approx \gamma_{MHD}/(n_{stab}/n_1) \tag{15c}$$

with the notation above, except that now γ_{MHD} is understood to include the Center Cell mass.

Though this dispersion relation gives instability, for our parameters it turns out that, even for a short solenoid length L_c, the growth rate in equation (15*c*) is of order $<100\,s^{-1}$, or growth on a timescale of 10's of milliseconds. Thus it should not be difficult to control this growth by applying feedback in the End Plugs.

4.3. Conflicting requirements, possible solutions

In this section we discuss how expander design, mirror design and feedback design might mitigate all of the uncertainties concerning trapped particle instability using non-paraxial mirrors and feedback mentioned in [31]. The applicability of feedback depends on the growth rate, perhaps best suited to controlling residual trapped-particle activity, whereas non-paraxial effects can stabilize MHD without resort to kinetic stabilization and perhaps without invoking trapped particle instability since particles providing stability by visiting regions of good curvature near the mirror throats also bounce between mirrors, hence serving as passing particles connecting regions of good and bad curvature. We defer details to section 9, noting that feedback calculations mainly rely on linear stability theory calculable in principle, as is the case also in analyzing non-paraxial stabilization of $m = 1$ MHD modes [35, 36].

4.3.1. Expander design. The expander serves multiple functions—to isolate hot electrons, to provide MHD stabilization, to process fusion energy released as charged particles, and, in appendix B, to apply direct conversion of charged particle energy to electricity. Careful design will be required to accommodate all of these functions in a single device.

A mitigating factor may be the following. It may be possible to separate the Expander into two zones, one near the final mirror coil, serving to isolate hot electrons and provide MHD stability. Flaring flux aids MHD stabilization in this region, strongest for $N = 3$ in our model of section 4.1. But this extreme line curvature can cause large-orbit ions that try to separate from electrons that follow the field lines. Space charge due to charge separation would create an electric field that approximately causes ions to follow the bending paths of electrons, well enough to apply MHD stabilization. Charge separation is avoided if field lines are straight, corresponding to $N = 2$ in the model. Thus the ideal Expander design may have a stabilizer zone with $N = 3$ near the mirror, followed by a zone with $N = 2$. We will return to direct converter design in appendix B. Here we use results in section 4.1 to show that a two-zone solution may be feasible.

For startup with $P_{stab} = P_{ECH}$, inserting numbers in the analysis yielding equations (7)–(10) and anticipating $R_p = (3.5/B_p)$ based on results in section 5, we obtain

$L_{exp} \approx 40L_{ma} \approx 40R_p = (140/B_p)$ for $N = 3$, giving $L_{exp} = 6$ to 12 m for End Plug fields B_p for our reactor models with advanced magnet technology in section 7. This portion of the expander would serve as the MHD stabilizer. Ions flowing from the Center Cell where the fusion power is generated would leave the stabilizer zone with the full potential energy ($\Phi_p \approx 1$ MeV), ready for Direct Conversion in a second zone. If the second zone length were similar to the stabilizer zone, the overall Expander length 12 to 24 m would be 1 or 2 times the diameter of the Center Cell including the blanket in figure 3.

Whether $L_{mag} \approx R_p$ or a larger dimension is correct for the scaling $B \propto (L_{mag}/z)^N$ assumed here depends on the size of the mirror coil required to produce the useful confinement volume plus protection against heat and neutrons. Neutrons tend to be suppressed in the End Plugs by using negative hydrogen ions to create neutral beams. Heat shielding mainly concerns Bremsstrahlung radiation that we estimate to be manageable in the End Plugs (<1% of the the ECH power).

4.3.2. Mirror design. The simplest mirror configuration would be just two circular coils at optimum spacing, with access for beam injection at an angle sufficient to control AIC instability (see figure 4), but short and fat enough to provide non-paraxial stabilization, at least for the $m = 1$ mode. Skewed injection producing 'sloshing ions' also reduces MHD growth rates [31]. A corresponding design feature would be radial angles for beam injection shaping $n_p(r)$ to maintain end plugging and DCLC stabilization while flattening $n_p(r)$ to match ECH feedback control mentioned below (see also section 7.5).

4.3.3. Feedback. Feedback may be especially applicable to the KSTM since feedback is only required in the small volume of the End Plug. A particularly simple method would be Post's proposal using pulses of pressure generated by pulses of ECH power [37]. Pulsing could be accomplished by modulation of the end-plugging ECH power source, analogous to audio modulation on an FM carrier frequency. Feedback sensing is not required, since stabilization follows from the Matthieu equation that also explains why oscillation of its fulcrum can make a pendulum stand on end [38] (see equation (2) in Post [37]). It may even be possible to stabilize MHD itself [37], there being no obvious limit on the modulation frequency required, the limit being instead a limit on the magnitude of pulsed power to match perturbation amplitudes. The pulsed power contribution should be much less than the steady state ECH power required for end plugging, and in any case power dissipation only adds to heating.

5. How stabilizing ion cyclotron modes determines radial dimensions

Kinetic microinstability in mirror devices is due to two departures from an isotropic Maxwellian distribution of ion velocities. One is due to mirror confinement of the ions, which can be described by different temperatures perpendicular and parallel to **B**. Modes mainly due to temperature anisotropy require finite parallel wave number $k_\parallel$ and are hence subject

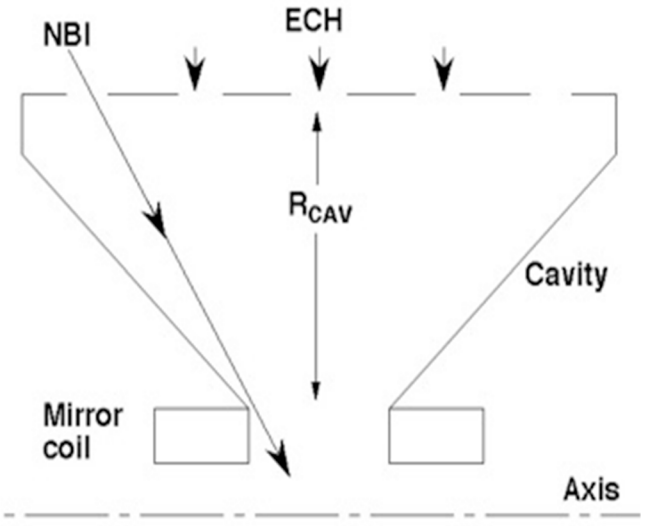

Figure 4. Sketch of an End Plug with a cavity to confine ECH, shaped to fit End Plug coils with access for ECH ports and skewed neutral beam injection. The cavity radius is 1 m for reactors using Next Generation magnet technology in table 2.

to stabilization by Landau damping that can be enhanced by injecting neutral beams at a skewed angle, as in figure 1. That Landau damping works at low density was demonstrated in the Baseball I experiment, which could be fully stable [39, 40]. At high density, the main mode of this type is the Alfven ion cyclotron (AIC) mode [20], which appears to have been mitigated by skewed beam injection in GDT [6, 7] but which remains on our list of subjects for further study in section 9.

Here we will focus on the drift cyclotron loss cone (DCLC) mode with $k_\parallel = 0$, hence not subject to Landau damping so that stability must be achieved by other means. The DCLC instability is a byproduct of a different departure from a Maxwellian due to the 'ambipolar' electrostatic potential plotted in figure 1. This potential, whose peaks in the End Plugs confine ions in the Center Cell, also ejects low energy ions out of the plugs toward the end walls. It is the 'ambipolar hole' due to this absence of low energy ions that drives DCLC, with one additional requirement. Namely, as already noted, the DCLC persists because it is a 'flute-like' mode with $k_\parallel = 0$, not suppressed by Landau damping. Then we should average the velocity distribution over $v_\parallel$, the relevant 'hole' being a hole in $v_\perp$ in the averaged distribution $\int dv_\parallel f(v_\parallel, v_\perp)$ [41].

In all high density experiments to date, the DCLC has been eliminated by the presence, inside the mirror confinement region, of a low temperature plasma partially filling the ambipolar hole to an amount correctly predicted by theory [42]. Ions filling the ambipolar hole escape freely, carrying away an energy per ion of order Φ_p that increases as temperatures increase, thereby accounting for the relatively poor energy confinement in these experiments.

According to theory, an End Plug of sufficient radial dimension no longer requires filling the ambipolar hole. The theoretical reason is that the flute-like 'drift waves' yielding DCLC instability are quantized with azimuthal wave numbers $k_\theta = m/r$. The DCLC instability only occurs when these

quantized electron drift waves that depend on the plasma radius are able to resonate at the ion cyclotron frequency, which introduces the ratio R_p/ρ into the criterion for stability, for plasma radius R_p and ion Larmor radius ρ (not to be confused with ρ as mass density in MHD theory).

That increasing the plasma radius does require less filling of the hole has already been demonstrated, in the range $R_p/\rho = 1.6$ to 6 [43]. Stability with an empty ambipolar hole is predicted for a plug radius $R_p > A_1$ (50ρ) and an adjustable parameter A_1. We obtain [42]:

$$R_p = A_l(50\rho) = 0.22A_l(E_o^{1/2}/B_p) \tag{16a}$$

$(\omega_{pi}/\omega_{ci})^2$	10^2	10^3	10^4	10^5
A_l	0.12	0.2	1.2	0.8

(16*b*)

In equation (16*a*), units are E_0 in keV and the mirror midplane field B_P in tesla. Equation (16*b*) is obtained as follows. Since the goal is small end plugs, a small value of R_p is advantageous. We note that R_p in equation (16*a*) is shorthand for $R_p = [d(\ln n_p)/dr]^{-1}$, allowing for various n_p profiles as needed to optimize DCLC stabilization versus control of trapped particle instability in a narrow pedestal extending from the end walls to the Center Cell, but not constrained by a tendency of the density profile to flatten in the interior of the Center Cell, as discussed in section 7.5.

Thus, though connected, we can think of $n_p(r)$ in the End Plug and $n_c(r)$ in the Center Cell pedestal as independent control knobs serving independent purposes. In this regard, we should treat equation (16*b*) as a necessary but perhaps not sufficient condition to achieve stable End Plugs, unless also the AIC mode is stable. Since it appears that it is the DCLC mode that is most responsive to the End Plug radius, as guidance we will use the table in equation (16*b*) which was obtained by fitting the theoretical DCLC stability curves in [42] (reproduced as figure 17 in [20]), which explains experiments to date as noted above. It is equation (16*b*) that we will use to determine the minimum radius of End Plug plasmas. It is the experimental confirmation of this criterion when the ambipolar hole is fully emptied that will be one of the main goals of suggested future experiments in section 8. Absent cooling by plasma filling the ambipolar hole, the required beam current is small—perhaps 5 A compared to 600 A available in the stream-stabilized 2XIIB experiment [44].

6. Why tandem mirrors favor high ion temperatures

The immediate goal of pure fusion research must be to compete with coal for the large power plants likely to be needed even as solar power and renewables continue to grow. Many fusion advocates have imagined fusion development via a sequence of applications, first hybrids using DT 14 MeV neutrons to breed fuel for fission reactors, followed by DT pure fusion power plants because DT is easiest to burn at low temperature, and finally followed by DD or other 'advanced fuels' not requiring the breeding of tritium from lithium.

As we show in this Section, tandem mirror pure fusion reactors are different in that even for DT they work best at the high ion temperatures that are also the realm of advanced fusion fuels. Then End Plugs adequate for DT are also adequate for advanced fuels, with a longer Center Cell. In this section and section 7, we will illustrate why this is so, for two example fuel cycles. Since high fusion power gain in a tandem mirror requires near ignition in the Center Cell, we omit the 'aneutronic' $p^{11}B$ fuel cycle that will not ignite according to Nevins [45]. We will also omit pure D^3He reactors (for which fuel is scarce on Earth). We will focus on DT reactors and the much-studied Catalyzed DD fuel cycle in which T and ^3He produced by DD reactions are recovered and fed back as fuel in the Center Cell, with no requirement for breeding tritium in the blanket, and very few 14 MeV neutrons if active means of ejecting T are employed to suppress DT reactions (see section 9.3.1) and all escaping T is allowed to decay to ^3He before reinjection.

6.1. Ignition in a tandem mirror

Experience suggests that loss cone turbulence discussed in section 5 cannot be tolerated so that, either End Plugs fail, or they can be designed so that end losses depend only on classical processes that are calculable. For this reason, here we will define ignition in terms of classical end losses only, with some justification discussed in section 7.7, but still highlighting radial transport as an important issue in section 9, along with some remaining uncertainty in the conditions for stability against the AIC loss cone mode.

6.2. Achieving ignition in steady state

With the above definition, the condition for steady state ignition can be written as:

$$n_1 n_2 \langle\sigma v\rangle f_c E_{fus} = (n_{ci}^2 \Phi_p / n_c \tau_i) + [\text{Radial loss} + \text{Radiation}] \tag{17a}$$

$$n\tau_i = n\tau_{ii}(\Phi_i/T_{ic})\exp(\Phi_i/T_{ic}) \tag{17b}$$

$$n\tau_{ii} = A^{1/2} 1.6 \times 10^{16} T_{ic}^{3/2} \tag{17c}$$

where n_1 and n_2 are fuel densities, n_c is the electron density, $\langle\sigma v\rangle$ is the fusion reaction rate and E_{fus} is the fusion energy and f_c is the fraction in charged particles. Here and hereafter we use collision rates in Dolan [46], already employed in equation (2*b*), with atomic number A and Coulomb logarithm given by $(15 + \ln T) = 20$, valid within 10–20% for densities $10^{19\text{–}21}$ m^{-3} and 50 keV $< T <$ 250 keV.

We will find that the required (Φ_i/T_{ic}) is about the same for all cases and Φ_p is not directly dependent on T_{ic}. Consequently, optimization with respect to end losses typically consists of minimizing radiation (and/or radial transport) and maximizing the product $\langle\sigma v\rangle n\tau_{ii}$. Since $\langle\sigma v\rangle n\tau_{ii}$ steadily increases with T_{ic} well above 100 keV (even for DT), we take the highest possible T_{ic} consistent with avoiding excess electron radiation in the Center Cell and End Plugs giving $T_{ic} = 150$ keV as a good choice for all reactions.

Hence we assume $T_{ic} = 150$ keV in the remainder of this paper. That $T_{ic} > 100$ keV is always favored for mirrors has

been a persistent fact beginning with simple mirror reactors in the 1950s [20].

7. Reactor examples

In this section, we consider a simple model to assess reactor prospects for our improved KSTM. We average over radial profiles, giving average densities, reaction rates and end losses, as if n, T etc were constant across the profile. That this is a reasonable approximation for tandem mirrors follows from the decoupling of end losses and radial losses. Radial profiles in an operating regime dominated by end losses can be shaped by neutral beam injection, which also serves as a 'limiter' defining the maximum radius of confinement short of the actual wall.

7.1. End plug design

Given DCLC stability, the maximum electron temperature T_{ep} that can be sustained in an End Plug must equate electron particle loss to ion loss, to achieve ambipolar outflow to the end walls. We neglect Center Cell losses and balance losses from an End Plug alone. We assume hydrogen neutral beams ($A = 1$) giving $n_i = n_e \equiv n_p$ in the End Plug. We obtain:

$$n_p^2(1/n\tau_{ii}(E_o)) + n_p^2\left(1/n\tau_{ie}\left(T_{ep}\right)\right) + n_p n_c(1/n\tau_{ie}(T_{ec})) = n_p^2\left(1/n_p\tau_e\right) \tag{18a}$$

$$n\tau_{ii}(E_o) = 1.6 \times 10^{16} E_o^{3/2} \tag{18b}$$

$$n\tau_{ie}(T_e) = 5 \times 10^{17} T_e^{3/2} \tag{18c}$$

$$n_p\tau_e = 4 \times 10^{14}\,[T_{ep}^{3/2}(\Phi_p/T_{ep})\exp(\Phi_p/T_{ep})] \tag{18d}$$

Anticipating $(n_p/n_c) \approx 5$, $T_{ep} = 250\,\text{keV}$ and $T_{ec} = 100\,\text{keV}$, the electron terms on the left hand side of equation (18*a*) sum to less than half of the ion term. Then dropping these electron terms, multiplying the ion scattering term by 3/2 and equating the result to the right hand side, we obtain:

$$30E_o^{3/2} \approx T_{ep}^{3/2}(\Phi_p/T_{ep})\exp(\Phi_p/T_{ep}) \tag{19}$$

where the factor $30 \approx (2/3\ m_H/m_e)^{1/2}$ and the right hand side is the Pastukhov $n\tau$ formula for electrostatic confinement applied to electrons [19], Φ_p being the total potential drop from the End Plug to the end wall.

We also require:

$$(\Phi_p - \Phi_{mirr}) \leqslant E_0(R_M - 1) \tag{20}$$

Equation (20) describes ion confinement in the mirror, Φ_{mirr} being the potential at the mirror throat. Equation (20) is derived as follows. Due to the constancy of the magnetic moment μ, mirror confinement of ions in the End Plug can be represented as the potential energy difference at the mirror, given by $(\mu\Delta B)_{max} \approx E_o(B(z) - B_p)/B_p = E_o(R_M - 1)$, with mirror ratio R_M. Mirror confinement of ions is opposed by the positive ambipolar potential difference $\Delta\Phi$ (from midplane to the mirror) that confines electrons. Ion confinement fails if $\Delta\Phi > (\mu\Delta B)_{max}$, giving equation (20).

Simultaneous solution of equations (19) and (20) determines the ratios (E_0/T_{ep}) and (Φ_p/T_{ep}) as functions of R_M. For example, 24 T magnets give $B_p = 12$ T with $R_M = 2$. Substituting $R_M = 2$ into $\Delta\Phi = E_0\ (R_M - 1) > E_o$ gives $T_{ep} = 0.25\ E_0$. We will take $E_0 = 1$ MeV, the beam energy under development for ITER [21], and we note that some exploration of parameters shows little benefit from higher beam energy. Then we obtain $\Phi_i = 0.25E_0\ln(n_p/n_c) = 400$ keV with $n_p/n_c = 5$, which will turn out to be adequate for a KSTM using 1 MeV neutral beams. Thus we will assume for all reactor cases below:

$$E_o = 1\,\text{MeV};\quad T_{ep} = 250\,\text{keV};\quad T_{ic} = 150\,\text{keV};$$
$$\Phi_p = 1100\,\text{keV} \tag{21}$$

The required neutral beam deposition is just the current given by multiplying the ion term on the left hand side of equation (18*a*) by the End Plug volume V_p, and also the charge e to give equivalent amperes. Again taking the electron terms to be about half of the ion term, we obtain:

$$I_{ion} = 3/2V_p\{en_p^2(1/(1.7 \times 10^{16}E_o^{3/2})\} \rightarrow 5V_p n_{p20}^2 \quad \text{amps} \tag{22}$$

where we round up the coefficient to 5. At 1 MeV, ions are deposited by proton ionization with cross section $\sigma_{ion} = 2 \times 10^{-21}$ m^2 [47]. The required equivalent neutral beam current to deposit this much current in the plasma depends on the quantity $2n_pR_p\sigma_{ion}$. We obtain:

$$2n_pR_p\sigma_{ion} = 0.4n_{p20}R_p \tag{23a}$$

$$I_{NBI} = I_{ion}/(0.4n_{p20}R_p) \rightarrow I_{ion} \tag{23b}$$

In equation (23*b*), the arrow applies if $(0.4n_{p20}\ R_p) > 2$ indicating that all energetic neutrals are deposited within a distance R_p.

We use equation (16*a*) to write R_p as:

$$R_p = 0.22A_1(E_o/B_p)^{1/2} = (3.5/B_p) \tag{24}$$

with $E_o = 1000\,\text{keV}$ from equation (21) and hereafter we take $A_1 = 0.5$ leaving some margin against DCLC requirements in equation (16*b*). We write n_p in terms of the pressure parameter β_p, giving:

$$\beta_p = 0.04n_{p20}(E_o + T_{ep})/B_p^2 = 50(n_{p20}/B_p^2) \tag{25a}$$

$$n_{p20} = 0.02\beta_pB_p^2 \tag{25b}$$

where we use $(nT/2\mu_o) = 0.04\ n_{20}T$, again with parameters in equation (21). Given n_p, we take the Center Cell density to be $n_c = 1/5n_p$ which optimizes confinement by equations (1*a*) and (17*a*). Applying equations (24) and (25*b*) to P_{ECH} in equation (4*b*) with $T_{pe} = 250\,\text{keV}$ in equation (21) gives, with $(T_{ep} - T_{ec}) \approx T_{ep}$:

$$P_{ECH} = (40.5n_{p20}^2)V_p = 4.4\beta_p^2B_p \tag{26}$$

This assumes negligible loss by synchrotron radiation, given by:

$$P_{syn} = 0.006 V_p\,[n_{p20} T_{ep} \gamma_L^2 B_p^2]\ \text{MW} \tag{27a}$$

$$= (2.2 n_{p20} B_p^2) V_p \tag{27b}$$

where, in equation (25*a*), $\gamma_L = [1 + (T_{ep}/m_e c^2)]^{1/2}$ is the Lorentz factor giving the relativistic correction [48], giving equation (27*b*) for $T_{ep} = 250\,\text{keV}$.

Synchrotron radiation must be reduced by enclosing the plug region inside a metal cavity. A sketch of the cavity is shown in figure 4, depicting a cavity shaped to fit around the End Plug mirror coils. These coils serve as entry ports to the cavity that joins the Center Cell to the Expander (not shown).

For a fully closed cavity, only a fraction of $P_{syn} \ll 0.1\%$ is absorbed in the cavity wall [49] (reproduced in [46], figure 3F6). Our main concern is leakage of synchrotron power through open ports, mainly ECH injection ports. The magnitude of the problem can be assessed by calculating the power ratio P_{syn}/P_{ECH}. Using equations (25*b*), (26) and (27*b*), we obtain:

$$(P_{SYN}/P_{ECH}) = (2.2 n_{p20} B_p^2/40.5 n_{p20}^2) = 3.0/\beta_p \tag{28}$$

From equation (28), we see that, for $\beta_p = 0.9$ in reactor examples below, a good design limiting synchrotron leakage to 10% of the ECH power would require a leakage no greater than (10%/3) $\beta_p = 3\%$, including any leakage by propagation through the mirrors into the Center Cell and Expander. Parameters fitting this requirement can be obtained using the arrangement shown in figure 4. ECH ports similar to those for ITER are located in the outer boundary of a cylindrical cavity, radius R_{cav}. Making the outer cavity width $1.5R_{cav}$ as shown leaves room for skewed injection of neutral beams as in figure 1. Tapering the cylinder to converge on the inner edge of mirror coils leaves room outside the cavity, on the Expander side, to supply cooling and current for the mirror coils, entering through a conical space between the tapered cavity and Expander fitted to the mirror throat (not shown).

The arrangement in figure 4 provides an ample area to install ECH ports, given by $A_{cav} = 3\pi w R_{cav} = 3\pi R_{cav}^2$. We note that the power density through ECH ports is limited, being 150 MW m^{-2} in ITER. Ignoring leakage by propagation and using the ITER limit and equation (26), we require:

$$(A_{port}/A_{cav}) P_{syn} = 3.3 (A_{port}/A_{cav}) P_{ECH} = 0.1 P_{ECH} = 0.1 A_{port} (150\,\text{MW m}^{-2}) \tag{29a}$$

$$A_{cav} = 3\pi R_{cav}^2 = (3.3/15)(4.4 \beta_p^2 B_p) = \beta_p^2 B_p \tag{29b}$$

$$R_{cav} = 0.3\,\beta_p B_p^{1/2} \tag{29c}$$

7.2. Designing for high Q

We characterize reactor performance by the fusion power gain Q, given for tandem mirrors by [20]:

$$Q = (P_{fusion}/2P_{plug}) = (V_c n_1 n_2 \sigma v E_{fus})/(2P_{plug}) \tag{30}$$

In the numerator, V_c is the Center Cell volume; n_1 and n_2 are the fuel densities; σv is the fusion reaction rate in the Center Cell; and P_{plug} is the plug injection power (neutral beams plus ECH). It will turn out that the net beam power is only a fraction of the ECH power, making it useful to account for beam power by its ratio to ECH power. Then we can rewrite Q as:

$$Q = (P_{fus}/2P_{plug}) \equiv L_c C\ [F/(1 + ((P^*_{NBI} + P_{EDGE})/P_{ECH})] = L_c C\ [F/(2\ + (P^*_{NBI}/P_{ECH})] \tag{31a}$$

$$C = (V_c/2L_c V_p) = (1/2A_2)(R_c^2/R_p^3) \tag{31b}$$

$$F = (n_1 n_2/n_c^2)(n_c/n_p)(\sigma v (E_{fus}/T_{ep}) n \tau_{ee}) \tag{31c}$$

In equation (31*a*), P^*_{NBI} is the net neutral beam power after 80% recovery of un-deposited power by direct conversion, as discussed in appendix B.1, and $P_{EDGE} = P_{ECH}$ is extra power applied to a Center Cell 'scrape-off' layer as it passes through the End Plug, in order to insure that this scrape-off layer can prevent the penetration of cold neutrals into the hot End Plug plasma where cold neutrals causing charge exchange could kill the End Plug. In equation (31*b*), the scaling factor is $A_2 = (L_p/R_p)$. In equation (31*c*), we set $T_{ep} - T_{ec} \approx T_{ep}$.

7.3. Fuel choices

As noted in section 6, we will consider two fuel options, designated as:

DT	D and Li fuel, by breeding T from Li in the blanket
Cat. DD	DD, catalyzed by re-injecting reaction products

To reduce neutrons, for the Cat. DD fuel cycle we will assume that tritium produced by DD reactions is stored to produce ^{3}He so that only ^{3}He is re-injected (perhaps controversial, as discussed in appendix A.5). For these fuels, the radiation terms can be assumed small in the ignition condition, equation (17*a*), which we rewrite as:

$$1/4 n_c^2 \langle \sigma v \rangle_{DT} f_c E_{fus}(\text{DT}) = (n_c^2 \Phi_p/n_c \tau_i)\text{DT} \tag{32a}$$

$$1/2 n_c^2 \langle \sigma v \rangle_{DD} f_c E_{fus}(\text{DD}) = (n_c^2 \Phi_p/n_c \tau_i) \quad \text{Cat DD} \tag{32b}$$

$$n\tau_i = A^{1/2}(1.6 \times 10^{16} T_{ic}^{3/2})(\Phi_i/T_{ic}) \exp(\Phi_i/T_{ic}) \tag{32c}$$

$$\Phi_i = T_{ep} \ln(n_p/n_c) \tag{32d}$$

where again f_c is the fraction in charged particles (20% for DT, 94% for Cat. DD neglecting residual DT reactions) and equation (32*c*) combines equations (17*b*) and (17*c*). Using parameters in equation (21) and nuclear parameters in Dolan [46], we can solve equations (32*a*) and (32*b*), giving approximately the same values for both cases, from which we take $n_p/n_c = 5$ and $\Phi_i = 400\,\text{keV}$ as anticipated in section 7.1.

Simplifying approximations include the following. We ignore radial losses by turbulence, consistent with our definition of ignition in a tandem mirror in section 6. The density n_c is the electron density. We ignore end losses due to reaction products so that n_c is also the sum of hydrogenic fuel ion densities, all with unit charge so that an electron–ion pair takes away their temperatures (which we ignore) but also the much larger

Table 1. Comparison of fusion fuels ($T_{ic} = 150$ keV).

Fuel	DT	Cat. DD
σv ($\times 10^{-22}$ m^3 s^{-1})	7.3	≈0.34
n_p/n_c	5	5
(τ_i/τ_{ii})	40	40
E_{chg} (MeV)	3.5	20.5
E_{fus} (MeV)	17.6	22
F	5.6×10^{-3}	5.1×10^{-4}

potential energy Φ_p, with a lifetime equal to that for the escape of D and T that we take to be the same for each, given by $(n_c\tau_i/n_c)$. We also ignore losses associated with fuel management, including alpha ash removal for the DT fuel cycle and tritium ejection to suppress 14 MeV neutron production in our version of the Cat. DD fuel cycle. The required auxiliary power is probably small, as discussed in section 9.3, the greater effect being some reduction in the plasma heating factor f_c in table 1 below. Calculations in section 9.3.1 lead us to omit altogether plasma heating by tritium in the Cat. DD cycle, a small effect since most of the heating is by D^{3}He reactions.

To justify dropping radiation, we assume that the Center Cell wall is designed to reflect most of the synchrotron radiation. The ratio of Bremsstrahlung to the fusion power is given by the following, for Cat. DD (the worst case):

$$\begin{aligned}(P_{Brem}/P_{DD}) &= Z_{eff}(3\times 10^{-21}T_e^{1/2}(1+2(T_{ec}/m_ec^2))\\ &\quad /\left(1/2\langle\sigma v\rangle_{DD}21\,000\right)\\ &< 0.17Z_{eff} = 0.17\left[\left(1+4f_{He}\right)/\left(1+2f_{He}\right)\right]\end{aligned} \tag{33}$$

The Bremsstrahlung formula is taken from Dawson with an approximate relativistic correction [50], with $T_{ec} < T_{ic} = 150$ keV and $\langle\sigma v\rangle_{DD} = 3.4\times 10^{-23}$ [46]. Here $Z_{eff} = 1$ for pure DD fuel is increased by $f_{He} \equiv (n_{3He}/n_e)$ due to re-injecting ^{3}He, for which we speculate $f_{He} \ll 1$ due to radial losses of higher-Z ions.

The actual value of T_{ec} is uncertain. Assuming that $T_{ec} < T_i$ for all fusion reaction products and also for T_{ic}, all ions transfer energy to electrons at the same rate, aside from a mass factor A, given by $n\tau_{ie} = A5\times 10^{17}T_{ec}^{3/2}$ from equation (18c), while the typical fuel ion lifetime is given by $n_c\tau_i \approx 10^{21}$ required for ignition against end loss, this being the lifetime for electrons also, assuming ambipolarity. Ignoring radiation and equating just these rates gives $(T_{ic} - T_{ec})/(5\times 10^{17}T_{ec}^{3/2}) = \Phi_i/10^{21}$, where $\Phi_i = \Phi_p - \Phi_c = 700$ keV, hence $\Phi_c/T_{ic} = (700/150) = 4.7$. We obtain roughly $T_{ec} \approx T_{ic} = 150$ keV. If this were the actual value including radiation and radial loss, the ECH power required in steady state would be reduced by a factor $(T_{ep} - T_{ec})/T_{ep} = 0.4$ giving a higher Q. However, as $T_{ec} \approx T_{ic}$ does not account for radial loss and it does not apply during start up, we will ignore this benefit in estimating reactor requirements.

Table 1 summarizes results up to this point. For Cat DD, we assume that all ^{3}He (both directly from DD and from the decay of T) is re-injected until it burns up, giving an effective fusion energy per DD reaction that is the sum of 3.7 MeV from DD, and 18.3 MeV from D^{3}He (roughly half from the ^{3}He reaction product and half from T decay).

Here, $E_{chg} = f_cE_{fus}$ in equations (32a) and (32b), giving simply $E_{chg} = 3.5$ MeV for DT-generated alpha particles, and the sum of charged particle reaction product energies for DD and D^{3}He for the Cat. DD cycle but omitting a net 0.5 MeV from the (T,p) branch if DT is suppressed by ejecting T as discussed in section 9.3.1. In this, we are treating only the DD reactions in equation (32b) but adding to the direct DD fusion energy release that of the associated ^{3}He as if ^{3}He reacts instantaneously as a simple way to represent a steady state Cat. DD cycle in which all ^{3}He (including that produced T decay) is burned up by repeated ejection (at the ends or radially) and re-injection (probably radially) until all is consumed. For Cat. DD we also neglect DT reactions as if T were ejected instantaneously. Active methods to remove tritium are discussed in section 9.3.1.

7.4. Reactor parameters

Separating Q into factors F and C in equation (31a) serves to separate what can be achieved by design, through the geometric factor C, from fuel properties contained in F. Given F, we now ask how to choose C so as to maximize Q. Equation (31b) gives, with $A_2 = 2$:

$$C = (R_c^2/4R_p^3) = 0.093B_p^3 \tag{34}$$

$$L_C = (Q\,/\,\mathrm{CF})\,[1 + ((P_{edge} + P^*_{NBI})/P_{ECH})] \propto 1/B_p^3 \tag{35}$$

In equation (34), the scaling comes from fixed R_c and $R_p \propto B_p^{-1}$ from equation (16a); and we choose a Center Cell radius $R_c = 4$ m for all cases. In equation (35), we use C to determine the Center Cell length L_c, using equation (31a).

7.5. Mapping magnetic flux

While fixing $R_c = 4$ m will turn out to give interesting reactor examples, confining a Center Cell plasma of radius 4 m by End Plug plasmas with radius $\ll 1$ m in these examples requires explanation. Magnetic flux in the Center Cell must match that in the End Plug. To minimize cost, we would like to utilize the high-β capability of mirrors to obtain pressure parameters $\beta_p = (2\mu_o p_p/B_p^2) \approx \beta_c \approx 1$ giving $(B_p/B_c) \approx (p_p/p_c)^{1/2} \approx 5$ for $p_p \propto (E_o + T_{ep})$ and $p_c \propto (T_{ic} + T_{ec})$ with numbers in equation (19) and $T_{ec} = 100$ keV. If B_c fills the Center Cell, for $R_c = 4$ the flux $\pi R_c^2B_c = 16\pi B_c \gg \pi R_p^2B_p$, indicating that pressure has crushed flux into a pedestal at $r = R_c$. The pedestal thickness Δ_{mag} is given by:

$$2\pi\Delta_{mag}R_c\langle B_c\rangle \approx \pi\Delta_{mag}R_cB_c = \pi R_p^2B_p \tag{36a}$$

$$\Delta_{mag} \approx (R_p^2B_p/R_cB_c) = (12.5/B_pR_cB_c) \tag{36b}$$

$$(\Delta_{mag}/R_c) = (12.5/R_c^2B_p) = (0.8/B_p) \ll 1 \tag{36c}$$

In equation (36b), we use $R_p = (3.5/B_p)$ from equation (24), giving equation (36c) evaluated for $R_c = 4$ m on the far right hand side.

Equation (36c) indicates a flat pressure profile in the Center Cell inside $r < (R_c - \Delta_{mag})$ while a steep tokamak-like

'pedestal' should form within the thickness Δ_{mag}. Exploring how a pedestal might be sustained was the main mission of the SYMTRAN code [15], which, even with a model for ETG transport of heat and particles, found solutions with flat pressure profiles out to the pedestal.

SYMTRAN results are summarized in section 7.7. Here we note that the natural tendency toward flat pressure profiles stabilizes the interior against MHD interchange, even as $B_c(r)$ goes to zero there, and the field curvature is stabilizing where this pressure enters the field near the mirror coil. Thus instability in this transition from solenoid to mirror, included in equation (6), only concerns the pedestal where curvature becomes destabilizing as field lines straighten out to join the solenoid. Estimating $(L_{tr}/R_{curv\ tr}) \approx 1$ and $\langle\beta_c\rangle \approx 0.5$ in the pedestal justifies our approximating the transition term equal to the End Plug term in equation (8). Note that, since any instability would occur far from the mirror, this argument holds for any R_p no matter how small. That ballooning is unlikely also is discussed in [20]. Verifying these conclusions is an important item in our Issues List in section 9.

It is important to note that the density profile in the Center Cell is relatively independent of that in the End Plug, an important point in designing the Center Cell to optimize radial confinement while designing the End Plug to stabilize DCLC modes, as discussed in section 5. At $\beta_c \approx 1$ in the Center Cell interior, all of the End Plug profile is mapped into the pedestal profile, the only constraint being that the stable End Plug also provides sufficient axial confinement everywhere. Thus the End Plug density can be flat or not as best suits End Plug stability, while the Center Cell naturally develops a flat interior as found in STYMTRAN.

7.6. Example reactors

The results above yield the following formulary for reactor design. We take $E_0 = 1$ MeV, $T_{ep} = 250$ keV, $T_{ic} = 150$ keV for all cases, from equation (21). We obtain:

$$R_p = 3.5/B_p;\ R_c = 4;\ R_{cav} = 0.3B_p^{1/2};\ P_{ECH} = P_{edge} = 3.49B_p$$

$$P_{fus} = 2QP_{plug} = 2QP_{ECH}\left[2 + 0.8\left(1 - 0.4n_{p20}R_p\right)\right];$$
$$V_p = \left(270/B_p^3\right)$$

$$L_c = Q(23.6/FB_p^3);\ C = 0.093B_p^3;\ B_c = 3n_{c20}^{1/2} = 0.2B_p$$

$$(E_{mag})_{vac} = \pi R_c^2 L_c (B_c^2/2\mu_o) = 0.02(L_c B_c^2)\ \text{GJ}$$

$$n_{p20} = 0.02\beta_p B_p^2;\ P_{ion} = 5V_p n_{p20}^2;\ P_{NBI} = \left(P_{ion}/f_B\right);$$
$$\rho_p = \left(0.14/B_p\right)$$

$$f_B = 0.4n_{p20}R_p;\ (\omega_{pi}^2/\omega_{ci}^2)_p = 2 \times 10^4 (n_{p20}/B_p^2)$$

Here we have combined quantities to exhibit the scalings with B_p. Note that $P_{fus} \propto QP_{plug} \propto B_p$ includes P_{edge} and the neutral beam power with 80% conversion of un-deposited power as mentioned earlier.

We will now apply this formulary and table 1 to consider 4 reactor examples. These examples reflect the strong influence of B_p on the Center Cell length L_c ($\propto 1/B_p^3$) while the fusion power only grows as $P_{fus} \propto B_p$. In table 2, B_p is the field at the mirror midplane, probably requiring at least double that at the mirror throat ($B_{mirr} > 2B_p$ for mirror ratio $R_M > 2$) in order to satisfy equation (20). The actual value requires detailed End Plug design, an important item in our Issue List. The only difference between DT and Cat. DD is through $F_{DD} = 0.1\ F_{DT}$.

To emphasize the strong effect of B_p, in table 2 we list 3 levels of magnet and gyrotron technology: one that can use ECH and the 1 MeV neutral beams being developed for ITER, labeled Existing; one using Next Generation magnet and gyrotron technology already under test on a scale sufficient for End Plugs, cited in [12]; and one for Futuristic technology building on cutting edge research on small 50 T magnets and 1 THz gyrotrons, which we represent as a base case with $B_p = 19$ T, with the benefit of extending this to 24 T indicated by arrows. For all cases we take $\beta_p = 0.9$, giving as the minimum field on axis $(1 - \beta_p)^{1/2}B_p = 0.3B_p$ for vacuum field B_p. That MHD-stable mirror-confined plasmas can achieve $\beta \approx 1$ was demonstrated in the 2XIIB experiment [51]. The GDT has achieved $\beta \approx 0.6$ with circular coils [6, 7]. In the Center Cell we calculate $\beta_c = 1$ for the maximum interior pressure and maximum B_c at the wall, as discussed in section 7.5.

The powers listed in table 2 assume 40% conversion of heat energy to electricity and 50% direct conversion of charged particle energy delivered to the Expanders. For the Cat. DD fuel cycle, it is assumed that tritium is stored to decay into ^{3}He before being re-injected, in which case neutrons contribute only 6% of the power, also in calculating the neutron wall load. The Nuclear Proliferation aspects of storing tritium are discussed in appendix A.5. We ignore heat recovery from the Direct Converter.

Lifetimes listed in table 2 are those for end loss from the Center Cell, with ion energy lifetime τ_E, ion particle lifetime τ_p (same for electrons for ambipolar flow) and ion scattering time τ_{ii} (Center Cell), giving $(\tau_p/\tau_{ii}) = (\Phi_i/T_{ic})\ \exp\ (\Phi_i/T_{ic})$ and $(\tau_p/\tau_E) = (\Phi_p/3T_{ic})$ for $T_{ec} = T_{ic}$. For comparison with 50 GJ in ITER, we list the magnetic energy $(E_{mag})_{vac}$ as if B_c filled the entire volume, with a radius $\approx (R_c + \Delta_B)$ to accommodate the blanket and shield between the coils and first wall (with $\Delta_B = 2$ m for DT, 1.5 m for Cat. DD).

The main message from table 2 is the significant improvement as the End Plug magnetic field is increased, first for DT with its higher value of F, but also for Cat.DD fuel as magnet technology improves. One sees large improvements both in the compactness of reactors and in their plant efficiency η_{eff} (listed with Net Electric power). But even the long reactors with lower magnetic energy (=cost) might compete. For all cases the Center Cell magnet technology is available today.

7.7. Radial losses, summary of SYMTRAN results

Table 2 shows that, if all losses were end losses, a KSTM could produce 1000 MWe in a DT reactor with magnetic energy storage of 6 GJ compared to 50 GJ in ITER, suggesting a sizeable reduction in reactor cost compared to tokamaks.

Table 2. Tandem mirror power reactors.

Technology Fuel	Existing DT	Next generation		Futuristic Cat. DD
		DT	Cat. DD	
Q/η_{eff}	10/22%	20/32%	10/29%	15 → 20/40%
Fusion power, MW	950	3700	1760	4280 → 7180
Net. Elec., MWe	210	1170	510	1540 → 2800
L_C, m	215	55	270	100 → 68
Neutron wall load, MW m^{-2}	0.15	2.1	0.015	0.1 → 0.25
Bmirr, T (minimum)	12	24	24	38 → 48
B_p, T	6	12	12	19 → 24
B_c, T	1.2	2.4	2.4	3.8 → 4.8
$(E_{mag})_{vac}$, GJ	5	6	28	29 → 32
C	20	160	160	1400
F, 10^{-4}	50	50	5	5
R_p/R_c, m	0.6/4.0	0.3/4.0	0.3/4.0	0.18/4.0
R_{cav}, m	0.6	1.0	1.0	1.2 → 1.3
n_{p20}	0.65	2.6	2.6	6.5 → 10.4
τ_p/τ_E	2.9	2.9	2.9	2.9
τ_p/τ_{ii}	40	40	40	40
P_{ECH}, MW	21	42	42	66 → 84
P_{NBI}, MW	17.5	17.5	17.3	17.4
P^*_{NBI}/P_{ECH}	0.26	0.18	0.18	0.15

Even our 1500 MWe Cat. DD reactor requires only 30 GJ magnetic storage.

These results depend crucially on our conclusion in section 7.5 that pressure buildup in the Center Cell yields a large stable volume at constant pressure and negligible magnetic field, surrounded by a pedestal containing all of the magnetic flux joining the Center Cell to the End Plugs. And that radial heat transport in the pedestal is acceptable.

We first show that classical heat transport into the pedestal is much less than end losses. Using equation (36*c*) and $\rho_{ic} = (0.08/B_c) = (0.4/B_p)$ for deuterium, we obtain:

$$(\Delta_{mag}/\rho_{ic})^2 = [(0.8R_c/B_p)/(0.4/B_p)]^2 = 64 \qquad (37)$$

Then, taking $\chi_{ii} = \rho_{ic}^2/\tau_{ii}$ for ion–ion classical heat transport across the pedestal thickness Δ_{mag}, we obtain, using equations (36*c*) and (37) and $(\tau_i/\tau_{ii}) = 40$ from table 1:

$$(P_{radial})_{class.}/P_{ends} = [(2\pi\Delta_{mag}R_c)(\chi_{ii}/\Delta^2_{mag})]/(\pi R_c^2/\tau_i)$$
$$= (2\Delta_{mag}/R_c)(\rho_{ic}^2/\Delta^2_{mag})(\tau_i/\tau_{ii}) = (1/B_p) \qquad (38)$$

Turbulent losses were included in SYMTRAN [15]. This code was a reactor version of the TAMRAC code [52] and TMT code [28] used to simulate results in TMX and TMX-U. The SYMTRAN simulations reported in [15] employed a critical-gradient model of ETG turbulence, taken to be:

$$\chi_{ETG} = C_{ETG}(T_{ec}^{3/2}/B_c^2)\,[\left|\mathrm{d}\ln T_{ec}/\mathrm{d}r\right| - L_{crit}^{-1}] \qquad (39a)$$

$$L_{crit}^{-1} = 3/2\left|\mathrm{d}\ln n_c(r)/\mathrm{d}r\right| \qquad (39b)$$

with $C_{ETG} = 0.1$ fitted to Tore SUPRA tokamak results with poloidal field replacing B_c [53]. Adding this χ_{ETG} to the classical χ's for ions and electrons (and 1/4 χ_{ETG} to particle diffusion) yields $Q = 10$ for a DT reactor 100 m in length with B only 0.5 T [15], similar to the Existing Technology case in table 2. The average Q was reduced from 20 to 10 due to low frequency oscillations of all parameters. These oscillations, which could be suppressed by auxiliary heating giving the same $Q = 10$, were attributed to a thermal instability due to the fact that T_{ec} also served as the End Plug temperature, hence not likely in an updated SYMTRAN using our new idea to decouple T_{ep} from T_{ec} as noted in section 3.2.

8. Next step experiment

Results above show that our new version of the KSTM tandem mirror can lead to attractive fusion reactors despite end losses in these machines, and that a design space exists for which end plugging only involves calculable processes, aside from issues with trapped particle modes. In this section we describe an experiment to verify these claims, including the stabilization of trapped particle modes by feedback if that proves necessary.

The experiment we have in mind would minimally include one End Plug connected to a magnetic expander on one side and some means of blocking plasma leakage out of the opposite end, similar to the GDT facility that inspired Post's invention of the KSTM. The goal would be first to resolve all issues concerning End Plugging, as a precursor to a full tandem mirror experiment in which radial transport in the Center Cell could be studied as the remaining physics issue of interest. This separation of issues is possible in tandem mirrors because the straight solenoid itself is a relatively benign plasma container, all unfavorable effects of magnetic design being localized to the End Plug and the transition where End Plug flux straightens out of join the solenoid.

The GDT has obtained what, for mirror devices, is a record thermal electron temperature of 1 keV. Our reactors require 250 keV. Here we explore what would be needed to reach 20 keV as a convincing milestone. The scope and cost can be fairly modest due the advances in magnetic technology that greatly reduce the size and cost of End Plug magnets and associated ECH power and neutral beam power if ion cyclotron modes are eliminated as predicted in section 5.

While we have not done a detailed design of such an experiment, its outlines are clear, as follows. For concreteness, we draw on engineering learned from fusion facilities in the past. As a starting point, one might choose 80–120 keV neutral beams like those constructed for MFTF and TFTR [54]. We will find that only one 5 A (0.4 MW) beam might suffice for the new experiment, if we also inject ECH. The 110–140 GHz gyrotron ECH frequency would be similar to that used in tokamaks. The mirror coils could be about the same as the circular 12 T NbSn coils constructed for MFTF-B, giving $B = 4$ T for a 3:1 mirror ratio. The beam power might be pulsed for 30 s as in MFTF.

Satisfying the conditions for ECH end plugging in section 3.2 favors 120 keV beams to achieve $T = 20$ keV for a mirror ratio $R_M = 2$, or 80 keV for $R_M = 3$ (coming from

the solution to equations (19) and (20)). Here we take 80 keV neutral beam injection (deuterium) and $R_M = 3$, giving the following results, derived below:

Machine Parameters
$B_p = 4$ T $B_{mirr} = 12$ T $n_{p20} = 0.5$
$R_p = 0.5$ m $I_{NBI} = 5$ A (all deposited)
110 GHz $P_{ECH} \approx 5$ MW
Performance:
$T_{ep} = 20$ keV; $R_p/\rho = 30$

The size is manageable. Overall dimensions of the containment vessel including the expanders would resemble just one section of the MFTF-B center cell.

That the powers listed here are much less than what would be obtained by scaling up GDT to a larger volume is due to the fact, discussed in section 5, that past experience from experiments in which the DCLC mode is stabilized by cold plasma filling the ambipolar hole is not a good guide if DCLC is fully stabilized. These numbers can be derived as follows. The parameters n_p, B_p and R_p are required to satisfy:

$$n_p(\sigma_i + \sigma_x)R_p = 1 \quad \text{all beam deposited} \tag{40a}$$

$$\beta_p = [0.04 n_{p20}(T_i + T_e)/B_p^2] < 1; R_p > 50 A_1 \rho_i \tag{40b}$$

Equation (40*a*) establishes efficient utilization of the neutral beams, subject in equation (40*b*) to limits on β_p and the DCLC stability condition, where σ_i (ionization) $= \sigma_x$ (charge exchange) $= 2 \times 10^{-20}$ m^2 at $T_i = 60$ keV produced by 80 keV beams [40]. Numbers above satisfy equation (36) with $\beta_p = 0.1$ and $\rho_i = 0.013$ m giving $A_1 = 0.7$ consistent with the DCLC stability condition in equation (16*b*). The beam current satisfies:

$$I = (e n_p V_p/\tau_{ii}) \tag{41}$$

Here $V_p = 2\pi R_p^3 = 0.8$ m^3 and $\tau_{ii} = 0.2$ s using equation (17*c*), giving $I = 3$ A, or 5 A with some contingency. This assumes ECH heating of the electrons to 20 keV and it ignores charge exchange.

In mirror devices, charge exchange losses in an outer shell of thickness ρ_i must be less than the ion deposition in this shell [54], giving the condition:

$$(I/e) n_p \sigma_i \rho_i > A_p\,[1/4 N_o n_p \sigma_x \rho_i F_o] \tag{42a}$$

$$F_o = \lambda_o/(\lambda_o + \rho_i) = v_o/[v_o + \rho_i(n_p(\sigma_x + \sigma_i))] \leqslant 1 \tag{42b}$$

Here N_o is the density of cold neutrals at the hot surface, with velocity v_o and mean free path λ_o. To reduce this to acceptable levels, we assume a cold plasma edge shielding the hot interior against an ambient density N_{amb}, sustained by ECH heating:

$$N_o = N_{amb} \exp(-n_p((\sigma v)_e/v_o)\Delta_{edge}) \tag{43a}$$

$$P_{ECH} = (T_e/T_i) IV + (2\pi R_p n_p \Delta_{edge} v_o T_o) \tag{43b}$$

Here $(\sigma v)_e \approx 10^{-14}$ m^3 s^{-1} is the ionization rate for 10 eV electrons (atom or molecule [43]), and $v_o = 3 \times 10^4$ m s^{-1} for 10 eV deuterium ions. Numbers above give $N_o = 0.001\ N_{amb}$ with $n_p \Delta_{edge} = 10^{19}$ giving $\Delta_{edge} = 0.2$ m and $P_{ECH} = 1.5$ MW for $N_{amb} = 3 \times 10^{16}$ (1 μTorr), or 5 MW for 3μTorr as in MFTF [40]. Recycling of neutrals from the wall is negligible if $f^*(\sigma_x/(\sigma_x + \sigma_i)) < 1$ where f^* is the number of cold neutrals returning when a hot neutral created by charge exchange strikes the wall [55]; hence not a problem in steady state reactor End Plugs where $\sigma_x/\sigma_i = 10^{-3}$ for 1 MeV ions, nor in the proposed experiment with $f^* \ll 1$ by gettering.

We imagine buildup to proceed as follows. First ECH creates a plasma (typically MW m^{-3} to initiate breakdown). This builds up a hot-electron, mirror-confined plasma serving as a target for neutral beam injection. If the cold neutral shielding works as expected, a hot core would be established with radius determined by beam angles, while ECH would continue to maintain an edge plasma shielding the hot interior. Modeling startup is a key issue in section 9.

9. Subjects for further study

In this section, we offer a list of topics for further study.

9.1. Plasma physics

(1) At the top of our list would be Fokker–Planck calculations of ECH runaway, discussed qualitatively in section 3.2. This problem, at the heart of the new concept explored in this paper, is complicated by issues of ECH propagation and absorption, listed also under issues of End Plug design in section 9.2.
(2) Second on our list would be more theory and simulations of trapped particle modes including Ryutov's Dissipative Sheath mode in an Expander but also including designs of Post's ECH feedback system discussed in section 4.3.3.
(3) Third on our list would be simulations of KSTM startup reaching a stable steady state in a new version of the SYMTRAN code, now including our new idea to decouple the End Plug and Center Cell electron temperatures that should avoid a thermal instability encountered in [15]. That the system is likely to be thermally stable can be seen as follows. Though runaway acceleration is faster the higher the energy, because electron cooling in the End Plug does not depend on T_{ec} in the Center Cell the main coupling is through n_c. But a loss of plugging causing n_c to decrease enters the loss side of the runaway condition as (n_c/T_{ep}), whereby a fall in n_c increases T_{ep} which restores end plugging.
(4) Fourth on our list would be radial transport in the Center Cell, using updated transport models in SYMTRAN together with a model of segmented end-plates unique to tandem mirrors, as mentioned in section 2. These studies might determine whether earlier evidence of radial transport in TMX-U [17], TARA [18] and Gamma 10 [24, 56] persists in the fully axisymmetric KSTM with end plates.
(5) Fifth on our list would be more theoretical work on the AIC instability at high beta in the End Plug, calculable

by linear theory. The AIC loss cone mode is not expected to be stabilized by a larger plasma radius measured in ion Larmor radii. Reducing $\beta_p = 0.9$ in table 2 to $\beta_p = 0.6$ in GDT would reduce $P_{fus} \propto P_{ECH}$ by a factor $(0.6/0.9)^2 = 44\%$.

(6) Sixth on our list would be application of PIC simulations to study turbulence in the End Plugs and Center Cell pedestal. In this regard, we note that the simple geometry of KSTM End Plugs may be a good candidate for a novel use of PIC simulation coding [57], in which semi-classical quantum PIC wavefunctions, explored by Dauger [58], could be employed to construct Hermitian eigenstates that could fully characterize sheath instability, AIC and other non-linear end-plug dynamics.

9.2. End plug design

(7) Conditions to prevent charge exchange losses in End Plugs need to be addressed. The likely result would be a requirement for an ECH-maintained halo to shield the hot plasma from surrounding cold neutrals, as discussed in section 8. Our estimates suggest that this may be supplied by the ECH power already included here as P_{edge} that would protect the End Plug as it flows from the Center Cell through the End Plug into the Expander.

(8) A corollary to Item (3) would be computer calculations of startup including ECH requirements to shield out cold neutrals. Beginning with TMX [10], starting up a tandem mirror has been relatively easy if End Plugs can build up. Then, gas fed to the Center Cell that is ionized by electron contact with the End Plug is very well confined by the large initial value of (n_p/n_c) appearing in the confining potential given by equation (1*b*).

(9) Detailed cavity design along the lines of figure 4 is needed, including mirror coil arrangements, ECH coupling and beam access, first for the experiment suggested in section 8. In this regard, for the Futuristic case in table 2, we estimated beam port requirements as follows. The required access for neutral beams is determined by the current density at the ion source and the angle of ion beam divergence determined by ion optics. The ion current density and minimum divergence achieved at the Lawrence Berkeley National Laboratory (LBNL) was about 10 A cm^{-2}, indicating a source size small enough that it is divergence that dictates beam dimensions for the ≈20 A requirements for all reactor cases above. The measured divergence was only 1° in agreement with calculations (see [54], figure 14). We find that this fits the 0.15–0.18 m plasma radius for the Futuristic case.

(10) Realistic designs of the Expander as an MHD stabilizer are needed, extending the work in [3] with attention to Direct Conversion, also. A crucial area needing simulation and analysis, mentioned in section 7.5, is the junction of the solenoid and mirror where the large Center Cell beta drops to a low value in the mirror throat.

9.3. Reactor

At the top of our list in this category would be issues of fueling and ash removal in DT reactors, and also tritium removal to suppress 14 MeV neutron production for the Catalyzed DD reactor example in section 7.

9.3.1. Tritium burnup and removal. Because tandem mirrors operate at high temperature, the normal assumption of a low burnup fraction allowing tritium produced by DD reactions to escape does not apply. A simple estimate of burnup and neutron production gives:

$$(n_T/\tau_T) = 1/2\,[1/2n_D^2(\sigma v)_{DD}] \tag{44a}$$

$$[1/2n_D^2(\sigma v)_{DD}]\,E_{chg} = \Phi_p(n_D/\tau_D) \quad \text{ignition} \tag{44b}$$

$$(n_T/n_D) = 1/2(\Phi_p/E_{chg})(\tau_T/\tau_D) \quad \text{burnup} \tag{44c}$$

$$(n_T/n_D)(\sigma v_{DT}/\sigma v_{DD}) \approx 0.5 \quad \text{neutrons} \tag{44d}$$

with lifetimes τ_T for tritium and τ_D for deuterium. Equation (44*a*) gives the tritium production rate and equation (44*b*) is the ignition condition. Combining gives the tritium burnup fraction in equation (44*c*). Taking $\tau_T \approx \tau_D$ and $\Phi_p = 1$ MeV from section 7 and $E_{chg} = 20$ MeV and $(\sigma v_{DT}/\sigma v_{DD}) = 21$ for the Cat. DD fuel cycle in table 1, we obtain $(n_T/n_D) \approx 0.025$, which gives 0.5 for the ratio of 14 MeV neutron production by tritium to 2.5 MeV neutron production by DD reactions.

Thus active methods must be used to remove tritium so as to suppress 14 MeV neutron production. One way to do this is to apply lower hybrid RF heating to tritium ions, shown to produce effective collisions by stochastic heating that can remove He ash in stellarator reactors with as little as 10 MW input [59]. Transport can also be enhanced by creating large Larmor orbits that enhance classical collisional transport [60]. The lower hybrid frequency is given by:

$$\omega_{LH} = \omega_{ci}[(\omega_{ci}/\omega_{ce}) + (\beta_i m_i c^2/2T_i)]^{-1/2} \tag{45}$$

In contrast with cyclotron resonance that does not distinguish between ions with the same (Ze/m) (e.g. D and ^{4}He), the term with β_i in […] is different for all ions and hence can be used to select for ejection any of the ions of interest here.

9.3.2. Helium ash removal. Both the Cat DD fuel cycle and the DT cycle produce ^{4}He which, as in tokamaks, must be removed, probably by active means using ejection methods discussed in section 9.3.1. For example, the helium buildup for DT can be calculated as follows. Comparing the rate of ^{4}He loss to its rate of production at ignition gives:

$$\begin{aligned}(n_{He_4}/n_{DT}) &= [1/4\,(\sigma v)_{DT}(n\tau)_{DT}]\,[(n\tau)_{He}/(n\tau)_{DT}] \\ &= (\Phi_p/E_\alpha)\,[(n\tau)_{He}/\,[(n\tau)_{DT}] \\ &> 0.3\,[(n\tau)_{He}/\,[(n\tau)_{DT}] \;>\; 0.3\end{aligned} \tag{46}$$

where $\Phi_p = 1.1$ MeV as in equation (32*a*) and the $n\tau$'s are products of density and particle confinement times by end loss, with $n_D = n_T = 1/2n_e$ and $\tau_D = \tau_D$ in $(n\tau)_{DT}$. We note also that it may be necessary to actively remove and re-inject

^{3}He in the Cat. DD fuel cycle so as to optimize the fuel mix, concerning, for example, the contribution of ^{3}He to the pressure that must be confined by the magnetic field.

Ash removal was also included in an early study employing a 2D Fokker–Planck code to couple 5 ion species to each other and to electrons, with the interesting conclusion that radial fueling from the edge might expel helium ash from the interior [61].

Other reactor subjects for further study are listed in appendices A and B.

10. Summary

This paper has presented an improved, simpler version of the tandem mirror concept based on ECH heating in the End Plugs but not requiring yin-yang mirrors or thermal barriers that complicated earlier high Q designs. In table 2, the new concept yields an attractive DT reactor using Next Generation technologies already under test, and a similar reactor burning Cat. DD fuel as magnet technology improves in the future.

As noted in the Introduction, in undertaking this paper our goal has been to show that all or most issues of the past concerning end plugging could be resolved in the Next Step end plug experiment discussed in section 8, leading to calculable designs in all respects except turbulent transport in the Center Cell that can only be resolved in a full tandem mirror with End Plugs employing design principles confirmed in the Next Step experiment.

We claim to have largely met our goal, by focusing first on how to design End Plugs large enough to avoid the DCLC ion cyclotron mode that can be stabilized in a device of sufficient size, measured in ion Larmor radii (an End Plug plasma with a radius around 25 ion Larmor radii). Obtaining stable ions was shown to lead to locally-Maxwellian electron distributions likely to be stable with the possible exception of trapped particle modes. Testing various means of stabilizing trapped particle modes, for example, by using the ECH heating system to provide feedback, would be an important element of a Next Step experimental program.

Our new version of Post's KSTM tandem mirror demands high performance of simple mirror machines serving as End Plugs, possible using a new idea based on strong ECH heating and advanced magnet and gyrotron technology. Renewed interest in tandem mirrors has been stimulated by results in the GDT simple mirror experiment at Novosibirsk that confirmed theoretical predictions of the benefits of utilizing expanding magnetic flux beyond the end mirrors, as shown in figures 1 and 2. The good curvature on expanding field lines can stabilize axisymmetric End Plugs similar to GDT. Also, expanding flux isolates the electron temperature in the End Plugs, allowing End Plug electron temperatures high enough to ignite DT and Cat. DD in the solenoidal Center Cell that serves as the fusion reactor.

A Next Step simple mirror experiment discussed in section 8 could achieve a thermal electron temperature $T_e = 20\,\mathrm{keV}$, midway between the record value of 1 keV achieved in GDT and the 250 keV needed for our reactor designs.

Acknowledgments

The authors thank Dmitri Ryutov, Arthur Molvik and the GDT Research Team for many useful discussions. We thank the reviewers for suggestions that have improved the paper. Finally, we wish to recognize the early work on symmetric tandem mirrors in the Phaedrus at the University of Wisconsin [62] and STM at the TRW Corporation [63].

Tributes

The authors are deeply indebted to their colleague Richard F. Post, inventor of the KSTM discussed here. Post initiated magnetic mirror fusion research in the United States and was still contributing original ideas upto the time of his death, April 7, 2015, at age 96. Also, the original proposal to apply Electron Cyclotron Heating to a Catalyzed DD tandem mirror was published by our Livermore colleagues in Fizika Plasmy [61], as a tribute to Academician G. I. Budker, following his death July 4, 1977. Budker was founding Director of the Budker Institute of Nuclear Physics, Novosibirsk, the location of the Gas Dynamic Trap experiment that inspired Post's KSTM. Finally we note with deep regret the recent death of our Russian colleague G I Dimov, whose independent invention of the tandem mirror at Novosibirsk helped to convince us that the idea was sound and in this way added support for undertaking tandem mirror research at Livermore.

Appendix A. Comparison of fusion fuel cycles, blanket design

In this appendix we sketch what blanket designs in figure 3 are appropriate for the Cat. DD cycle by comparison to D–T where tritium-breeding blankets are needed. For D–D, tritium breeding could be included in the blanket but it is not necessary. Economics will help decide what to do with neutrons.

A.1. Implications of tritium breeding: yes or no

If we do not need to breed tritium as required for the D–T fuel cycle, then the blanket can be simplified by not containing lithium, beryllium and some other low-Z elements that have neutron side reactions that produce tritium. The Cat. DD fuel cycle in table 2 does not require tritium breeding. This means the blanket can be virtually free of tritium production and handling. This should reduce the cost of the blanket and systems that otherwise would deal with tritium. However, since tritium is produced in the fusing plasma, there will be tritium-handling equipment. Further, since tritium readily diffuses through hot materials, the 'first wall' (the wall facing the plasma) and its cooling system would have to deal with tritium. This suggests separating the first wall cooling system from that of the blanket in order to obtain the advantage of a blanket not dealing with tritium. We discuss separating the first wall and blanket in section A.2.

A.2. First wall: integral or separate from blanket

The First Wall will be hot and any tritium in the chamber can readily diffuse into the first wall coolant. To get the 'tritium free' advantage of the blanket, the First Wall cooling system will need to be separated from the blanket's cooling system. This means the blanket and its associated systems will become simpler and lower cost if the blanket does not have to deal with tritium. Nevertheless we will have the design complication and increased cost of making the First Wall separate from the blanket in order to make it separate enough to avoid tritium issues. Designs will be needed before a quantitative assessment of the cost trade off of not breeding tritium can be made.

A.3. D–D versus D–T neutrons

Besides avoiding tritium breeding issues when using D–D reactions, the 2.5 MeV neutrons can be stopped with thinner, less massive blankets than for the case of 14 MeV neutrons from the D–T reaction. Still these blankets must both stop the neutrons, capture their useful energy at high enough temperature to produce useful power and they must attenuate gamma radiation enough to protect the superconducting magnets. The total blanket plus shield will be thinner for D–D reactions than for D–T reactions resulting in an economic advantage. The lack of dealing with tritium in the D–D blanket if we chose to forgo tritium breeding will further save cost.

A.4. Economics—what are the pros and cons of producing neutrons?

While the focus of this paper is pure fusion reactors, we note that avoiding the breeding of tritium or fissionable products produced by neutrons would forego a significant value of neutrons beyond that of their energy content. A hybrid KSTM, otherwise like the pure fusion designs in this paper, is the subject of [64].

Conversely, since advanced fuels produce more of their energy as charged particles rather than as neutrons, one might pose the question, 'Could we economically discard the thermal energy from neutrons and just direct convert the charged particle energy from advanced fuels?' The result might be interesting in that the challenging blanket design might turn into merely the design of an ordinary low temperature shield. Still we might want to recover in a thermal cycle the thermal energy on the first wall from radiation losses from the plasma and the energy in the direct converters not converted to electrical energy.

A.5. Nuclear proliferation

An important issue mentioned in section 7.6 is the nuclear proliferation implications of tritium produced in DD reactors if this tritium is stored long enough to decay into ^{3}He fuel. The quantity involved in storing 56 kg yr^{-1} of tritium from a 1000 MWe DD reactor for the 12.3 year half-life of tritium is about 1000 kg.

Even if storing tritium turns out to be unfeasible, so that one should instead re-inject tritium directly until all is consumed, the fact that tritium need not be bred in the blanket is still worth exploring—ultimately because deuterium is an inexhaustible fuel available to all. The possibility that there may be economic advantages for the Cat. DD cycle justifies trying to prove the feasibility of burning Cat. DD. Detailed multidisciplinary design studies of the various options brought up in this paper will quantitatively determine which is the best.

Appendix B. Direct conversion and expander design

In this appendix we discuss direct conversion of end leakage plasma in our version of Post's KSTM that can increase electrical power output and simultaneously provide design options to aid stability in multiple ways, both MHD and the control of radial transport discussed in section 2.

As noted in section 4.3, the design of the Expander that connects the tandem mirror to the direct conversion grid/electrode set can impact the stabilizing function. The value of direct conversion is somewhat marginal at the high Q of reactor designs in this paper. In section 7, we take a direct conversion efficiency of 50%. Despite the challenges, the potential to achieve 50% or greater direct conversion should be thoroughly explored in future work. We discuss some of these challenges in this appendix.

B.1. Voltage issues

Insulators can hold ~1000 kV m^{-1} (10 kV cm^{-1}100 kV) under practical conditions. For 100 kV systems sufficient for D–T fusion, the insulators have dimensions of ~0.1 m. Advanced fuels have energies requiring ~1 MV giving insulators ~1 m. Such insulators must be protected from 'seeing' charged particles, UV and x rays and from contamination by evaporated or sputtered metals. An example of such a 1 MV class insulator is discussed in a paper on a 1.6 MeV neutral beam injector with direct conversion [65]. A 1 MeV neutral beam injector for the KSTM will be made more energy efficient by direct conversion of the unused portion of the ion beam. An example will illustrate the point: a 20 A, 1 MeV negative ion beam can be passed through a neutralizer where roughly 5 A remain as negative ions, 10 A are singly stripped to neutrals and 5 A are doubly stripped or ionized to positive ions. The efficiency of producing neutrals is then 50%. If 70% of the ion energy is converted back to electricity, then to produce the 10 MW of neutrals requires 20 MW of prime power less the 7 MW of recovered power (5 MW $\times$ 70% for the positive ions and the same for the negative ions) so 13 MW are consumed, giving a 10/13 = 77% efficiency of producing neutrals. If 80% of recovered power is converted to electricity, then beam production is 83% efficient. An important technological issue is insulator design to hold off such high voltages as discussed in [65]. A beam direct converter was built [66] and tested [67] at 120 kV and 1 MW.

B.2. Grid power density limits

Plasma direct converters use grids to separate electrons from ions and collect the electrons on the grids. Such gridded systems are power limited to about 1 MW m^{-2} limited by radiation cooling keeping the grid temperature low enough to limit thermionic emission losses. The grid power limits will be discussed more fully in the next sections. The simplest direct converter has a single collector plate. However, efficiency can be increased by having a series of transparent tilted plates or collectors resembling Venetian Blinds that allow ions to pass in the forward-going direction but become opaque after reflection [68]. As noted below, a design study was carried out for power plant scale application and successfully tested.

B.3. Radial potential control

As was demonstrated in the TMX-U experiment [17], the end wall can be segmented into nested annuli each with a different potential applied. This was shown to suppress neoclassical radial losses, and the same technique could control the radial potential gradient (electric field) that might suppress radial losses in the Central Cell. The end walls composed of grounded 'grid wires' on a particular magnetic field line in open-ended systems sets a reference for the electrical potential, usually ground, called zero potential. However, it does not have to be zero. In fact this potential can be varied with radius.

When direct conversion of plasma end losses is implemented, we replace the end plates with a set of electrodes. The simplest form is to first have a grid that ends up collecting electrons, while the next grid is held sufficiently negative to reflect all electrons who experience multiple passes through the first grid until they are collected. The third and next electrode is a plate that is held positive to slow down ions and collect them. Usually this potential is slightly below the maximum potential of the axial confining potential of the tandem mirror. For KSTM reactors this potential might be of order ~1 MV. If we want higher efficiency we might employ Venetian Blind collectors, each held at a successively higher potential [68]. By tilting the Venetian Blind collectors, they easily pass ions of greater energy than the collector's potential (qV) but upon reflection the transparency becomes virtually opaque and they are collected. If the ions have enough energy they can pass on through successively higher potential collectors. A power plant scale direct converter of this type has been designed [69] where the efficiency of handling 1000 MW of power was estimated to be 59% and 65% for a two-stage and four-stage converter costing \$0.1/W of input power (1974\$). Also a gridded direct converter has been tested on the TMX experiment and obtained an efficiency of 48% [70].

The efficiency of such gridded direct converters for end loss plasma depends on many factors such as the potential structure in the tandem mirror, secondary electron and ion impact, secondary electron emission losses, gas ionization losses and the number of Venetian Blind collectors employed. 50% efficiency seems achievable. The electrodes can operate at such a high temperature that they can radiate the power that is not direct converted to electrical power to outer ground potential walls where thermal conversion can convert this power to electricity at >40% efficiency.

B.4. Grid heat load from kinetic stabilization augmentation

The kinetic stabilization effect discussed in section 4.1 arises from placing plasma in regions of favorable magnetic curvature in the expander so that it will out-weigh unstable regions. For the two-zone Expander in section 4.3, the stabilizer is the zone nearest to the final mirror coil. If the energetic outflow whose energy is to be direct converted is insufficient to produce stability, an augmented outflow could be implemented. One way to do this is to inject gas in a portion of the expander where it becomes ionized. Another way is Post's proposal to inject ions using low energy accelerators from the ends [1–3]. Either method adds to the heat load on the grids in the direct converter zone beyond the stabilizer zone.

Ions leaving the collector plate pass through the grids heating them, then reflect somewhere in the expander and come back through the grids and do this multiple times, thus increasing the grid heat load. Thermionic emission sets the power limit for radiation-cooled grids to ~1 MW m^{-2}. A larger expander would be needed to keep the heat load down to 1 MW m^{-2}.

This 1 MW m^{-2} limit is based on ions carrying most of the energy passing once through such grids. If the ions are reflected in the direct converter by a high voltage collector plate meant to recover energy from even higher energy escaping ions, then unfortunately the power is concentrated on the grids by the factor of how many passes are made before interception. We might be able to use direct-cooled grids such as water-cooled tubes to exceed thermionic emission-limited power and increase the power density. Grid dimensions are limited by space charge considerations.

Preferably, stabilizing plasma can be introduced at a potential just below that of the peak end cell potential. Then the direct converter collector plate can have its potential somewhat below this value and still perform well allowing only one pass through the grids. This gives us both stability and direct conversion, still, the expander will have to grow in size to keep the heat load down to 1 MW m^{-2}.

We might choose to segment the end walls into a number of annular zones as mentioned earlier. Each zone might have a different first-grid potential. The collector plate might have a lower potential or even zero for the outer zone where the energy of the leaking plasma is low and successively increased potential on inner zones where the leaking plasma ions are of higher energy. Such zoning is useful and likely even necessary to limit the electrical stored energy that can be discharged in a spark so as to limit damage from such sparking that is normal in electric power devices.

B.5. Conclusions

Simple direct converters that resemble gridded energy analyzers appear to be practical devices to convert leaking plasma energy to electrical energy at efficiencies greater than 50%

with the remaining 50% still available for the usual thermal conversion. Experiments have verified the performance at voltages of order 100 kV and 6 kW of power for 80 h. There will be mutually conflicting requirements for implementing kinetic stabilization and direct conversion that will have to be studied and verified by experimentation. Trade offs will have to be made. However, the performance of such implementation appears predictable.

References

[1] Post R.F. 2001 *Trans. Fusion Sci. Technol.* **39** 25
[2] Post R.F. 2003 *Fusion Sci. Technol* **43** 195
[3] Post R.F., Fowler T.K., Bulmer R., Byers J., Hua L. and Tung D. 2005 *Trans. Fusion Sci. Technol.* **47** 49
[4] Mirnov D.D. and Ryutov V.V. 1979 *Sov. Tech. Phys. Lett.* **5** 279
[5] Ryutov G.V. and Stupakov D.D. 1986 *Fiz. Plazmy* **12** 815
[6] Ivanov V.V. and Prikhodko A.A. 2013 *Plasma Phys. Control. Fusion* **55** 063001
[7] Bagryansky P.A. 2015 *Phys. Rev. Lett.* **114** 205001
[8] Dimov G.I., Zakaidakov M.E. and Kishinevskii V.V. 1976 *Fiz. Plasmy* **2** 597 (*Sov. J. Plasma Phys.* **2** 326)
[9] Fowler B.G. and Logan T.K. 1977 *Commun. Plasma Phys. Control. Fusion Res.* **2** 167
[10] Coensgen F.H. *et al* 1980 *Phys. Rev. Lett.* **44** 1132
[11] Ryutov D.D. 2005 *Trans. Fusion Sci. Technol.* **47** 148
[12] Whyte D. 2016 private communication
[13] Post R.F. 1987 *Nucl. Fusion* **27** 1579
[14] Simonen T. 2008 The Status of research regarding magnetic mirrors as a fusion neutron source or power plant *Lawrence Livermore National Laboratory Report* LLNL-TR-409570
[15] Taylor R.J. *et al* 1989 *Phys. Rev. Lett.* **63** 2365
[16] Hooper E.B., Baldwin D.E., Fowler T.K., Kane W.C. and Turner R.J. 1984 *Phys. Fluids* **27** 2264
[17] Hua T.K. and Fowler D.D. 2004 *LLNL Report* UCRL-ID-204783
[18] Post R.S. *et al* 1987 *Plasma Physics and Controlled Nuclear Fusion Research Proc. 11th Int. Conf. (Kyoto, 1986)* (Vienna: IAEA) p 251
[19] Pastukhov V.P. 1974 *Nucl. Fusion* **14** 3
[20] Fowler T.K. 1981 Mirror theory *Fusion* vol 1, ed E. Teller (New York: Academic) ch 5
[21] IAEA Vienna 2012 *Fusion Physics* ed M. Kikuchi *et al* (Vienna: IAEA) (www-pub.iaea.org/MTCD/Publications/PDF/Pub1562_web.pdf)
[22] Baldwin B.G. and Logan D.E. 1979 *Phys. Rev. Lett.* **43** 1318
[23] Dandl R.A. and Guest G.E. 1981 The ELMO Bumpy Torus *Fusion* vol 1, ed E. Teller (New York: Academic) ch 11
[24] Saito T., Kiwamoto Y., Tatematsu Y., Yoshimura Y., Takahashi T., Kasugai A., Kira F., Katanuka I., Yamaguchi N. and Tamano T. 1986 *Fusion Eng. Des.* **29** 3749
[25] Fowler T.K. and Rankin M. 1983 *Plasma Phys.* **4** 311
[26] Cohen R.H. 1983 *Phys. Fluids* **26** 2774
[27] Hiroe S. *et al* 1984 *Phys. Fluids* **27** 1019
[28] Mirin A.A., Auerbach S.P., Cohen R.H., Gilmore J.M., Pearlstein L.D. and Rensink M.E. 1983 *Nucl. Fusion* **23** 703
[29] Hinton F.L. and Rosenbluth M.N. 1982 *Nucl. Fusion* **22** 1547
[30] Ryutov D.D. 1987 Axisymmetric MHD stable mirrors *Proc. Intern. School of Plasma Physics* ed S. Ortolani *(Varenna, Italy, 1–11 September 1987)*
[31] Ryutov D.D., Berk H.L., Cohen B.I., Molvik A.W. and Simonen T.C. 2011 *Phys. Plasmas* **18** 092301
[32] Berk H.L. and Pratt J. 2011 *Nucl. Fusion* **51** 83025
[33] Berk H.L. and Lane B.G. 1986 *Phys. Fluids* **29** 3749
[34] Ryutov D.D. 2004 private communication
[35] Ryutov D.D. and Stupakhov G.V. 1985 *JETP Lett.* **42** 35
[36] Ryutov D.D. and Stupakov G.V. 1966 *Sov. J. Plas. Phys.* **12** 815
[37] Post R.F. 2010 *Fusion Sci. Technol.* **57** 335
[38] Ruby L. 1996 *Am. J. Phys.* **64** 39
[39] Damm C.C., Foote J.H., Futch A.H., Hunt A.L., Moses K. and Post R.F. 1970 *Phys. Rev. Lett.* **24** 495
[40] Post R.F. 1981 Experimental base of mirror-confinement physics *Fusion* vol 1, ed E. Teller (New York: Academic) ch 6
[41] Post R.F. and Rosenbluth M.N. 1966 *Phys. Fluids* **9** 730
[42] Baldwin D.E. 1977 *Rev. Mod. Phys.* **49** 317
[43] Correll D.L. *et al* 1980 *Nucl. Fusion* **20** 655
[44] Coensgen F.H. *et al* 1975 *Phys. Rev. Lett.* **35** 1501
[45] Nevins W.M. 1998 *Fusion Energy* **17** 25
[46] Dolan T.J. 1982 *Fusion Research* (New York: Pergamon)
[47] Sweetman D.R. 1973 *Nucl. Fusion* **13** 157
[48] Jackson J.D. 1998 *Classical Electrodynamics* 3rd edn (New York: Wiley)
[49] Miley G.H. 1976 *Fusion Energy Conversion* (Hinsdale, IL: American Nuclear Society)
[50] Dawson M.J. 1981 Advanced fusion reactors *Fusion* vol 1, ed E. Teller Chapter 16 453–500 (New York: Academic)
[51] Turner W.C. *et al* 1979 *Nucl. Fusion* **19** 1011
[52] Cohen R.H. 1979 *Nucl. Fusion* **19** 1295
[53] Horton W. 2003 Electron transport and the critical gradient *Review Talk* F11 4 DPP/APS Albuquerque
[54] Kunkel W.B. 1981 Neutral beam injection *Fusion* ed E. Teller (New York: Academic)
[55] Fowler T.K. 1975 *Plasma Phys.* **17** 583
[56] Mase A. *et al* 1991 *Nucl. Fusion* **31** 1725
[57] Fowler T.K. Speculations about plasma free energy, 50 years later *J. Plasma Phys.* accepted
[58] Dauger D.E. 2001 Semi-classical modeling of quantum mechanical multiparticle systems *PhD Thesis* Department of Physics, UCLA
[59] Grekov D.L. 2005 *Nucl. Fusion* **45** 751
[60] Chan V., Chiu Y.A. and Omelchenko S.C. 2001 Ion cyclotroinduced fast ion transport and plasma rotation in tokamaks *General Atomics Report* GA-A23659
[61] Logan B.G., Mirin A.A., Rensink M.E. and Fowler T.K. 1978 *Fiz. Plasmy* **4** 542 (1978 *Sov. J. Plasma Phys.* **4** 301)
[62] Herskowitz N. 1990 *Nucl. Fusion* **30** 1761
[63] Quan B.H. *et al* 1985 *Phys. Fluids* **28** 1503
[64] Ivanov A.A. *et al* An ECH driven high-field tandem mirror as a fusion-fission hybrid unpublished
[65] Moir R.W. 1994 *Fusion Technol.* **25** 129 (http://askmar.com/Fusion_files/1.6%20MeV%20Neutral%20Beam%20Direct%20Energy%20Conversion.pdf)
[66] Barr W.L., Doggett J.N., Kinney J.D. and Moir R.W. 1977 *Proc. 7th Symp. on Eng. Problems of Fusion Research (25–28 October 1977)* (http://www.askmar.com/Fusion_files/Beam%20Direct%20Conversion%20Engineering.pdf)
[67] Barr W.L., Moir R.W. and Hamilton G.W. 1982 *J. Fusion Energy* **2** 131 (*Proc. 8th Symp. on Eng. (San Francisco)*)
[68] Moir R.W. and Barr W.L. 1973 *Nucl. Fusion* **13** 35
[69] Barr W.L., Burleigh R., Dexter W.L., Moir R.W. and Smith R.R. 1974 *IEEE Trans. Plasma Sci.* **2** 71
[70] Barr W.L. and Moir R.W. 1983 *Nucl. Technol. Fusion* **3** 98 (http://ralphmoir.com/wp-content/uploads/2012/10/fusion-science-and-technology.pdf)